






Structure and mechanism of a eukaryotic ceramide synthase complex

Tian Xie[†] , Qi Fang[†] , Zike Zhang , Yanfei Wang, Feitong Dong  & Xin Gong^{*} 

Abstract

Ceramide synthases (CerS) catalyze ceramide formation via N-acylation of a sphingoid base with a fatty acyl-CoA and are attractive drug targets for treating numerous metabolic diseases and cancers. Here, we present the cryo-EM structure of a yeast CerS complex, consisting of a catalytic Lac1 subunit and a regulatory Lip1 subunit, in complex with C26-CoA substrate. The CerS holoenzyme exists as a dimer of Lac1-Lip1 heterodimers. Lac1 contains a hydrophilic reaction chamber and a hydrophobic tunnel for binding the CoA moiety and C26-acyl chain of C26-CoA, respectively. Lip1 interacts with both the transmembrane region and the last luminal loop of Lac1 to maintain the proper acyl chain binding tunnel. A lateral opening on Lac1 serves as a potential entrance for the sphingoid base substrate. Our findings provide a template for understanding the working mechanism of eukaryotic ceramide synthases and may facilitate the development of therapeutic CerS modulators.

Keywords ceramide; ceramide synthase; cryo-EM; Lac1; Lip1

Subject Categories Membranes & Trafficking; Metabolism; Structural Biology

DOI 10.15252/emj.2023114889 | Received 29 June 2023 | Revised 20 October 2023 | Accepted 24 October 2023 | Published online 13 November 2023

The EMBO Journal (2023) 42: e114889

Introduction

Ceramide is not only a building block of complex sphingolipids but also a critical signaling molecule in all eukaryotic organisms that regulates numerous cellular processes, such as apoptosis, senescence, proliferation, and differentiation (Hannun & Obeid, 2008, 2018; Gault *et al.*, 2010; Harrison *et al.*, 2018; Summers *et al.*, 2019). However, the aberrant accumulation of ceramide is a hallmark of numerous human metabolic diseases, such as obesity, diabetes, and cardiovascular disease (Hla & Dannenberg, 2012; Chaurasia & Summers, 2015, 2021; Havulinna *et al.*, 2016; Laaksonen *et al.*, 2016; Lemaitre *et al.*, 2018; Mantovani *et al.*, 2018, 2020; Summers, 2018; Karjalainen *et al.*, 2019; Hilvo *et al.*, 2020; Poss *et al.*, 2020a, 2020b; Choi *et al.*, 2021). Ceramide is mainly synthesized in the ER from the

reaction of a sphingoid base with a fatty acyl-CoA via sphinganine N-acyltransferases, also known as ceramide synthases (CerSs) (Pewzner-Jung *et al.*, 2006; Levy & Futerman, 2010; Mullen *et al.*, 2012) (Fig 1A). CerS enzymes are promising therapeutic targets for various metabolic diseases such as obesity, insulin resistance, cardiovascular diseases, and non-alcoholic steatohepatitis (NASH), as well as cancers (Park *et al.*, 2014; Brachtendorf *et al.*, 2019; Raichur, 2020).

CerS enzymes were first identified over 20 years ago in the budding yeast *Saccharomyces cerevisiae*, where two distinct members, Lag1 and Lac1, are required for acyl-CoA-dependent ceramide synthesis reaction (Guillas *et al.*, 2001; Schorling *et al.*, 2001). Both Lag1 and Lac1 catalyze the N-acylation of a sphingoid base [dihydro-sphingosine (DHS) or phytosphingosine (PHS)] with the preferred C26-CoA to generate C26-dihydroceramide or C26-phytoceramide (Guillas *et al.*, 2001; Schorling *et al.*, 2001). A later study revealed that a regulatory Lip1 subunit forms a complex with the catalytic subunit Lag1 or Lac1 and is required for CerS activity both *in vivo* and *in vitro* (Vallée & Riezman, 2005). Nevertheless, the exact role of Lip1 in the ceramide synthesis reaction is unknown, and no obvious homologs of Lip1 were found in mammals (Vallée & Riezman, 2005).

Mammals contain six distinct CerS isoforms (CerS1-6), each of which strongly favors a particular subset of acyl-CoA substrates with different acyl chain lengths varying between C14 and C26 (Venkataraman *et al.*, 2002; Guillas *et al.*, 2003; Riebeling *et al.*, 2003; Mizutani *et al.*, 2005, 2006; Laviad *et al.*, 2008). It has been clear that ceramide species with different acyl chain lengths execute distinct biological functions (Hannun & Obeid, 2011; Turpin-Nolan & Brüning, 2020). An 11-amino acid sequence, located between the last two transmembrane helices (TMs), has been shown to determine the acyl chain specificity of mammalian CerS (Tidhar *et al.*, 2012, 2018). However, the mechanistic details of how this region controls the acyl chain specificity await further investigation.

Members of the CerS family share a common multiple transmembrane TRAM-Lag-CLN8 (TLC) domain of ~200 residues, which is also found in other protein families (Winter & Ponting, 2002). A conserved stretch of 52 residues, called the Lag1p motif, is found within the TLC domain of the CerS family, but not in the other two TLC domain families (Jiang *et al.*, 1998; Winter & Ponting, 2002). Four highly conserved charged residues in the Lag1p motif, two histidine and two aspartate

Department of Chemical Biology, School of Life Sciences, Southern University of Science and Technology, Shenzhen, China

*Corresponding author. Tel: +86 75588018495; E-mail: gongx@sustech.edu.cn

[†]These authors contributed equally to this work

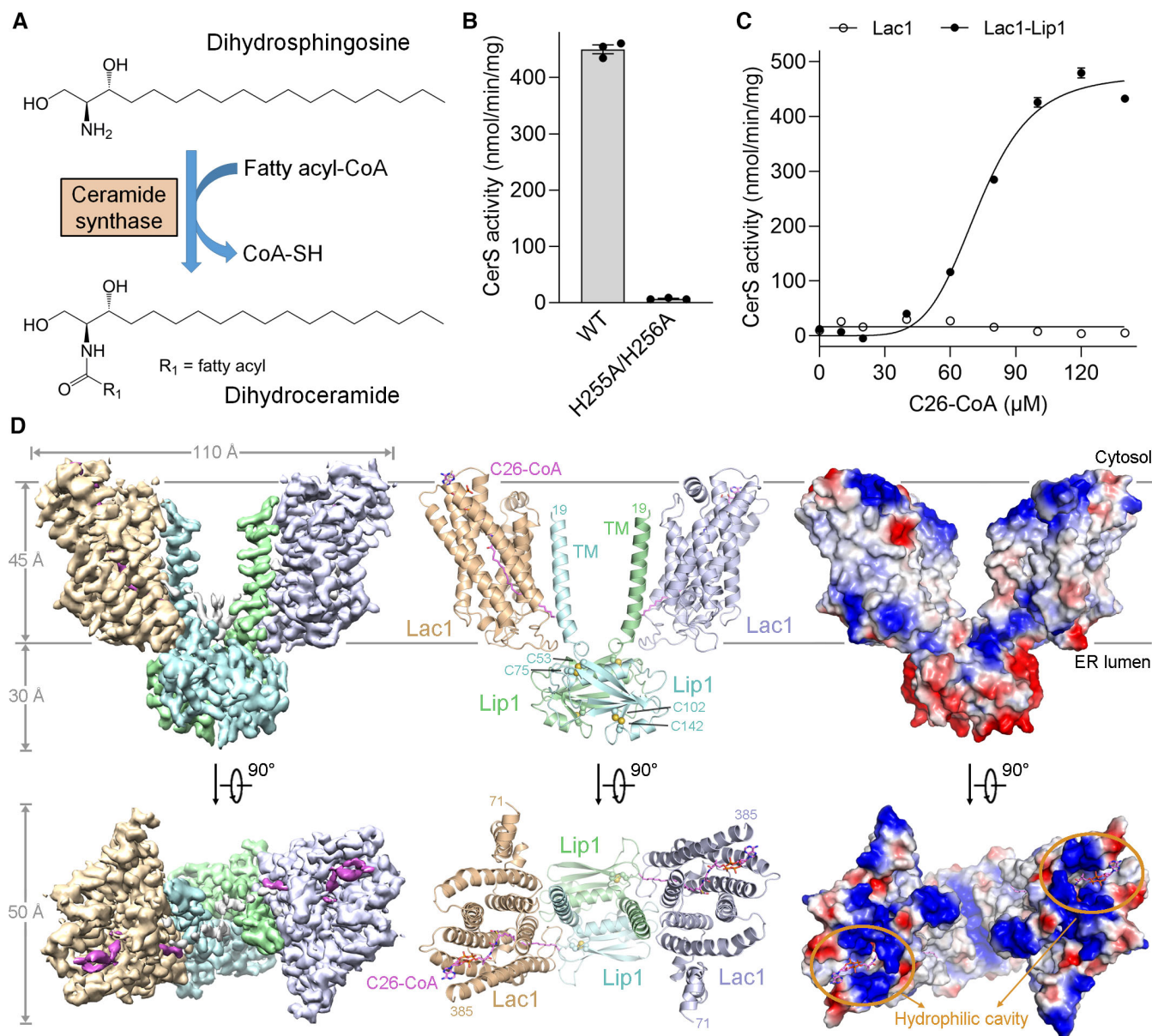


Figure 1. Biochemical and structural characterization of the yeast Lac1-Lip1 complex.

A Ceramide synthase (CerS) catalyzes ceramide formation via N-acylation of a sphingoid base with a fatty acyl-CoA. Dihydrosphingosine (DHS), a representative sphingoid base, was used to generate dihydroceramide in the activity assays in this study.

B Enzymatic activity of the wild-type (WT) Lac1-Lip1 complex and the catalytic mutant Lac1^{H255A/H256A}-Lip1 complex. Each data point is the average ± SEM of three independent experiments.

C CerS activity versus C26-CoA concentration for the Lac1 alone protein and the Lac1-Lip1 complex. The activity curve of the Lac1-Lip1 complex follows an allosteric sigmoidal equation with a K_{half} of $72.99 \pm 1.44 \mu\text{M}$ for C26-CoA and a V_{max} of $475.7 \pm 13.1 \text{ nmol/min/mg}$. Each data point is the average ± SEM of three independent experiments.

D Perpendicular views of the cryo-EM map, overall structure, and electrostatic potential surface of the C26-CoA-bound Lac1-Lip1 complex. Lac1 and Lip1 form a heterotetramer with a 2:2 stoichiometry. C26-CoA lies inside the Lac1 subunit and traverses the lipid bilayer. The two Lac1 subunits are shown in wheat and light blue, respectively; the two Lip1 subunits are shown in light cyan and light green, respectively; C26-CoA is shown in magenta. The two intramolecular disulfide bonds within Lip1 are shown in spheres. TM, transmembrane helix.

Source data are available online for this figure.

residues, have been predicted to be located in the active site of the CerS enzyme family (Kageyama-Yahara & Riezman, 2006; Spassieva et al, 2006) (Fig EV1). The lack of structural information regarding

CerS has largely limited the mechanistic understanding of CerS functions. In this study, we report the first atomic structure of a eukaryotic CerS, the yeast Lac1-Lip1 complex, bound with an acyl-CoA substrate

at an overall resolution of 3.09 Å, as determined by single-particle cryo-EM. We also established an *in vitro* biochemical assay to measure the CerS activity. Combined with structure-guided mutational analysis, our work serves as a foundation for understanding the structure–function relationship of eukaryotic CerSs.

Results

Biochemical characterization of the yeast Lac1-Lip1 complex

Yeast Lag1 (411 residues) and Lac1 (418 residues) share 73% sequence identity and appear to be functionally redundant proteins since single deletions caused no obvious defects in yeast (Jiang et al, 1998; Barz & Walter, 1999). The recombinant protein expression and purification of Lag1-Lip1 and Lac1-Lip1 complexes are described in detail in Materials and Methods (Fig EV2A). We employed an *in vitro* enzymatic assay, previously utilized for assessing the activity of serine palmitoyltransferase (SPT) complex (Li et al, 2021; Liu et al, 2023; Xie et al, 2023), to measure the activity of the purified CerS complexes. This was achieved by monitoring the release of free CoA-SH from the N-acyltransferase reaction (Fig 1A). In the presence of 100 μM DHS and 100 μM C26-CoA substrates, the catalytic activity of the Lac1-Lip1 complex could be readily detected (Fig 1B), whereas the activity of the Lag1-Lip1 complex was only around 5% of that of the Lac1-Lip1 complex (Fig EV2B). As negative controls, mutations of the two highly conserved histidine residues in the Lag1p motif of Lag1 or Lac1 to alanine (H255A/H256A) resulted in a complete loss of enzymatic activity of both complexes (Figs 1B and EV2B). Since the purified Lac1-Lip1 complex exhibited much higher enzymatic activity compared to the purified Lag1-Lip1 complex, we focused on the Lac1-Lip1 complex for the following biochemical and structural studies.

We measured the enzymatic activity of the Lac1-Lip1 complex with various concentrations of C26-CoA or DHS. The activity curve with different concentrations of DHS follows a Michaelis–Menten equation (Fig EV2C), whereas the activity curve with different concentrations of C26-CoA fits well with an allosteric sigmoidal equation (Fig 1C), suggesting that C26-CoA has a regulatory role on the complex. To investigate whether Lip1 contributes to the enzymatic activity of the purified complex, we expressed and purified the Lac1 subunit alone. The Lac1 alone protein was well-folded and exhibited a monodisperse peak in size-exclusion chromatography (SEC) (Fig EV2D), suggesting that Lip1 is not necessary for the proper folding of Lac1. No enzymatic activity was detected for Lac1 alone protein (Figs 1C and EV2C), supporting that Lip1 is essential for the enzymatic activity of the purified complex.

Structural determination of the Lac1-Lip1 complex

The structure of the Lac1-Lip1 complex was determined by single-particle cryo-electron microscopy (cryo-EM) in the presence of 0.5 mM C26-CoA substrate (Appendix Fig S1A–F). Representative 2D averages indicated a dimeric organization of the complex (Appendix Fig S1B). A density map of the Lac1-Lip1 complex was reconstructed to an overall resolution of 3.09 Å with an imposed C2 symmetry (Appendix Fig S1F). The EM map was of excellent

quality, enabling unambiguous model building for most of the protein regions and assignment of C26-CoA (Appendix Fig S2A–E, Appendix Table S1). The resolved structure reveals that the Lac1-Lip1 holoenzyme is a dimer of Lac1-Lip1 heterodimers (Fig 1D). In each Lac1-Lip1 heterodimer, a C26-CoA molecule lies inside the Lac1 subunit and traverses the lipid bilayer, with the CoA moiety facing the cytosol (Fig 1D).

The N-terminal 18 residues of Lip1 were invisible in the cryo-EM map (Fig 1D), probably owing to its intrinsic flexibility. The resolved Lip1 structure (residues 19–150) contains a single transmembrane helix (TM) and a luminal α/β domain consisting of five anti-parallel β-sheet strands and two α helices (Fig EV3A). The TM of Lip1 is responsible for the assembly of Lac1-Lip1 heterodimer, while the luminal domain of Lip1 mediates homo-dimerization (Fig 1D). A Dali (Holm, 2022) search for structural homologs of Lip1 in the Protein Data Bank (PDB) failed to identify any protein with a similar fold, implying that Lip1 represents a novel fold.

Two intramolecular disulfide bonds (Cys53-Cys75, Cys102-Cys142) were found within the luminal domain of each Lip1 subunit (Figs 1D and EV3A and B). We generated four single-cysteine mutants of Lip1 (C53A, C75A, C102A, C142A) and purified the mutated Lac1-Lip1 complexes (Fig EV3C). These four mutants resulted in greatly reduced expression levels, poor solution behavior in SEC, and less than 10% of the enzymatic activity of the WT complex (Fig EV3C and D). The results indicate that the two intramolecular disulfide bonds within the luminal domain of Lip1 are important for the proper folding and enzymatic activity of the complex.

The Lip1 homo-dimerization interface involves extensive interactions between the α1/β3/β4/β5 segments of both subunits (Fig EV3B). To investigate the functional impact of Lip1 homo-dimerization interface, we generated a four-point mutation of Lip1 (R78A/Y81A/Y125A/Y148A) (Fig EV3B). Although the mutated complex remained partially as dimer in SEC, this mutant displayed prominently reduced expression level, relatively poor solution behavior with broad SEC peak, and approximately 5% of the enzymatic activity of the WT complex (Fig EV3E and F). The data implies that the Lip1 homo-dimerization interface might also be important for the proper folding and enzymatic activity of the complex.

Lac1 encloses a conserved hydrophilic reaction chamber

Each Lac1 subunit contains eight TMs (TM1–TM8), with both N- and C-termini facing the cytosol (Fig 2A). Among the eight TMs of Lac1, TM3–TM8 constitute the TLC domain and TM1–TM2 are named as the N-terminal domain (NTD) (Fig 2A). The N-terminal 70 residues and C-terminal 33 residues of Lac1 were not resolved, indicating the high flexibility of these regions. The structure reveals three long luminal loops of Lac1, which connect TM1/2, TM3/4, and TM7/8, respectively (Fig 2A). In addition to the eight TMs, three short helices were resolved in the Lac1 structure, including one cytosolic helix (CH1) preceding TM1 and two luminal helices (LH1 and LH2) located within TM1/2 and TM3/4 loops, respectively (Fig 2A).

The TLC domain of Lac1 forms a large hydrophilic cavity within the membrane that is open to the cytosolic side (Figs 1D and 2B and C). The four highly conserved charged residues within the

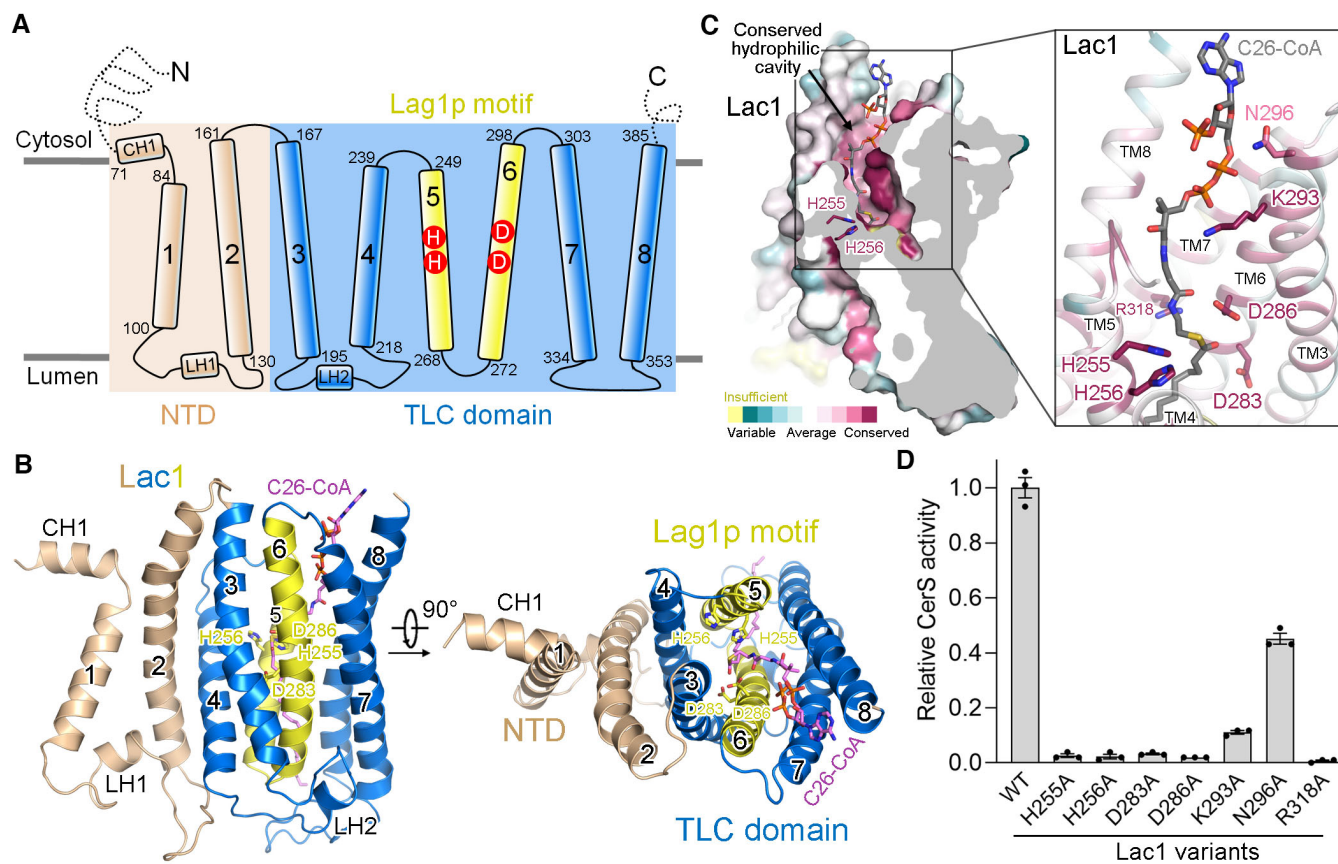


Figure 2. A conserved hydrophilic reaction chamber within Lac1.

A Schematic representation of the topology of Lac1. NTD, N-terminal domain; TLC, TRAM-LAG1-CLN8; CH, cytosolic helix; LH, luminal helix.

B Two perpendicular views of the Lac1 subunit. The NTD is colored wheat. The TLC domain is colored marine with the Lag1p motif shown in yellow. C26-CoA is shown in magenta sticks. The predicted catalytic histidine and aspartate residues in the Lag1p motif are shown in sticks.

C A conserved hydrophilic cavity within the TLC domain of Lac1. Lac1 is colored by the amino acid conservation scores calculated by ConSurf (Yariv *et al*, 2023) analysis of the yeast and human CerS members presented in Fig EV1. The conserved charged and polar residues within the hydrophilic cavity are shown in sticks. C26-CoA is shown in gray sticks.

D Functional characterization of the conserved charged and polar residues shown in panel (C) by CerS activity. The activities of Lac1-Lip1 variants were normalized relative to that of the WT Lac1-Lip1 complex. Each data point is the average \pm SEM of three independent experiments.

Source data are available online for this figure.

Lag1p motif (TM5-TM6) of Lac1, namely His255, His256, Asp283, and Asp286, are buried inside the cavity with their side chains facing the cavity (Fig 2B and C). The hydrophilic CoA moiety of C26-CoA binds within the cavity, placing the thioester bond of C26-CoA close to the conserved His and Asp residues (Fig 2B and C). These structural observations further support the possibility that the highly conserved His and Asp residues shared by CerS family enzymes are involved in substrate binding and/or catalysis and indicate that the acyl-transfer reaction occurs within the membrane.

To assess the function of residues within the hydrophilic cavity, we first made four single-point alanine mutations targeting the highly conserved His and Asp residues of Lac1 (H255A, H256A, D283A, D286A). All four single-point mutations did not affect the folding of the complexes (Appendix Fig S3A), but the purified mutants essentially lost the catalytic activity (Fig 2D). We also generated three other Lac1 mutants targeting the two other invariant charged residues and one less conserved polar residue within the

hydrophilic cavity (K293A, R318A, N296A) (Appendix Fig S3A). The enzymatic activity of the three mutants was severely impaired (Fig 2D). Together, these studies suggest that the charged and polar residues within the hydrophilic cavity are crucial for enzyme-catalyzed reactions, possibly due to their important roles in substrate binding and/or catalysis.

Acyl chain binding tunnel

The acyl chain of C26-CoA extends through the reaction chamber towards the ER lumen (Fig 3A). The acyl chain lies deep within a hydrophobic tunnel formed by TM4-TM8 of Lac1 and is coordinated by numerous hydrophobic residues lining the tunnel (Fig 3B and C). Four hydrophobic residues (Leu341, Phe343, Tyr348, and Ile352) in the last luminal loop (TM7/8 loop) of Lac1 and one hydrophobic residue (Phe40) in the TM of Lip1 make close contacts with the distal end of acyl chain, allowing the tunnel to

perfectly accommodate a 26-carbon acyl chain (Fig 3C). The activity of the Lac1-Lip1 complex was examined using a series of acyl-CoA substrates with shorter acyl chains (Fig 3D). The activity of Lac1-Lip1 complex in the presence of C24-CoA was only ~20% of that with C26-CoA as a substrate, and the activity obtained using C22- to C14-CoA was less than 5% of that with C26-CoA as a substrate (Fig 3D). Acyl-CoA molecules with shorter acyl chains cannot fully occupy the hydrophobic tunnel, which may explain the

molecular basis for the acyl chain-length selectivity of the Lac1-Lip1 complex.

In contrast to the highly conserved residues in the hydrophilic reaction chamber enclosed by Lac1, residues lining the acyl chain binding tunnel are less conserved in yeast and human CerS homologs, especially those near the distal end of the acyl chain (Fig 3E). This is consistent with the distinct acyl-CoA preferences of yeast and human CerS homologs. Ten Lac1 hydrophobic residues lining

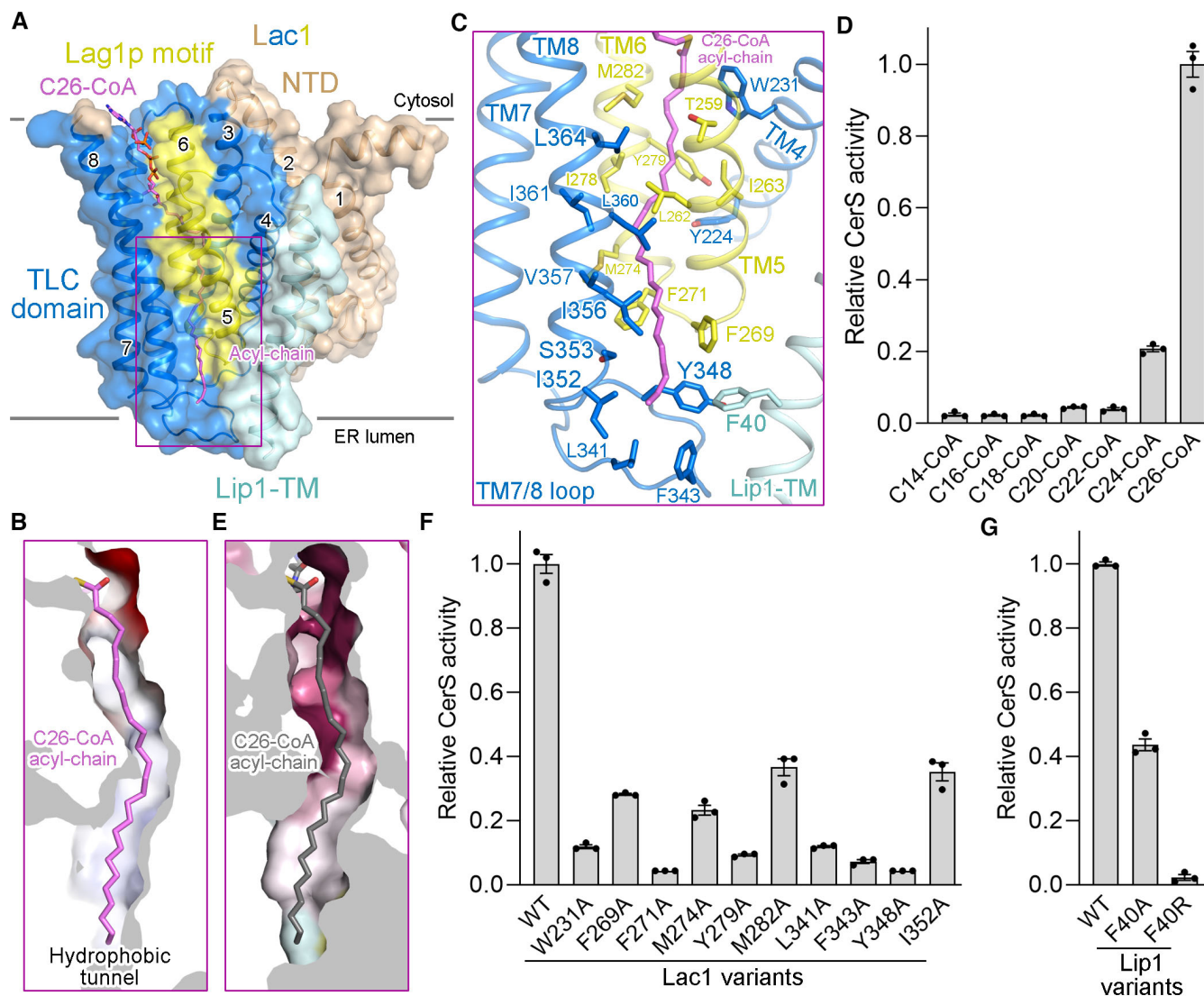


Figure 3. The acyl chain binding tunnel.

A C26-CoA is coordinated by the TLC domain of Lac1 and the TM of Lip1.

B A hydrophobic tunnel for C26-CoA acyl-chain binding in Lac1.

C A close-up view of the interactions between C26-CoA acyl-chain and the Lac1-Lip1 complex. The residues lining the acyl chain binding tunnel are shown in sticks.

D Acyl-chain selectivity of the Lac1-Lip1 complex revealed by CerS activity. Each data point is the average \pm SEM of three independent experiments.

E The distal end of the hydrophobic tunnel for C26-CoA acyl-chain coordination is not conserved. Lac1 is colored by the same amino acid conservation scores as in Fig 2C.

F, G Functional characterization of Lac1 (**F**) and Lip1 (**G**) hydrophobic residues for C26-CoA acyl-chain binding by CerS activity. Each data point is the average \pm SEM of three independent experiments.

Source data are available online for this figure.

the acyl chain binding tunnel were individually mutated to the less bulky residue alanine (W231A, F269A, F271A, M274A, Y279A, M282A, L341A, F343A, Y348A, and I352A). The mutated complexes were well-folded (Appendix Fig S3B), but their catalytic activity was drastically reduced (Fig 3F). Mutation of Phe40 of Lip1 to alanine or arginine (F40A, F40R) also preserved protein folding (Appendix Fig S3C), but led to ~60% or complete loss of catalytic activity, respectively (Fig 3G). Data on these two Lip1 mutants suggest that Lip1 can enhance the catalytic activity of the complex probably by engaging in Lac1 interaction and acyl chain binding, akin to the stimulatory role of small regulatory subunit in the human SPT complex (Li *et al*, 2021; Wang *et al*, 2021). In conclusion, these results support the importance of acyl chain binding residues for the optimal catalytic activity of the complex.

Interactions between Lac1 and Lip1

Lac1-Lip1 heterodimer is assembled mainly through the interactions between TM of Lip1 and TMs 2/4/5 of Lac1 (Fig 4A and B). The hydrophobic residues Ile20/Leu23/Val26 of Lip1-TM pack closely against Val239/Leu240 of Lac1-TM4 near the cytosolic side of the membrane (Fig 4B). Meanwhile, the hydrophobic residues Leu31/Ile34 and Leu33/Val37/Phe40 of Lip1-TM pack against Leu133 of Lac1-TM2 and Trp264/Phe269 of Lac1-TM5, respectively, near the luminal side of the membrane (Fig 4B). Moreover, the side chain of Lys41 in Lip1-TM forms a potential hydrogen bond with the main chain of Val268 in Lac1-TM5, further strengthening the Lac1-Lip1 TM interface on the luminal side (Fig 4B). We created two Lip1 mutants at the TM interaction interface, namely Lip1^{V37F/K41F} and Lip1^{V37Y/K41Y}. Our results indicate that both mutants partially impaired the formation of the complex between Lac1 and Lip1, providing evidence for the importance of the TM interaction interface in the formation of the Lac1-Lip1 complex (Appendix Fig S4A).

In addition to the interaction interface in the TM region, Lip1 also makes contact with Lac1 in the luminal region (Fig 4A and C). At the luminal interaction interface, Phe51/His52/Ser74 in the luminal domain of Lip1 and Asn342/Phe343 in the TM7/8 loop of Lac1 are very close to each other, with the side chains of His52 and Ser74 in Lip1 forming potential hydrogen bonds with the main chains of Phe343 and Asn342 in Lac1, respectively (Fig 4C). To explore the functional importance of the luminal interaction interface, we generated four Lip1 mutants (F51A, F51R, H52A, and S74F). The mutated complexes folded similarly as the WT complex, and these four mutants did not affect the binding between Lip1 and Lac1 (Appendix Fig S4B), indicating that the binding between Lip1 and Lac1 is

mainly contributed by the TM interaction interface. Mutation of Phe51 or His52 of Lip1 to alanine resulted in a ~60% reduction or essentially complete loss of catalytic activity, respectively (Fig 4D). Mutating Phe51 of Lip1 to a charged arginine or mutating Ser74 of Lip1 to a bulky phenylalanine also nearly abolished the enzymatic activity of the complex (Fig 4D). We also assessed the enzymatic activity of the Lac1-Lip1^{F51A}, Lac1-Lip1^{F51R}, Lac1-Lip1^{H52A}, and Lac1-Lip1^{S74F} mutants using C14- to C26-CoA substrates. Our data showed that the Lac1-Lip1^{F51A} mutant displayed similar acyl-CoA substrate selectivity as the WT complex, and the other three mutants were essentially inactive with all the acyl-CoA substrates tested (Appendix Fig S4C). These results suggest that the specific interaction of Lip1 and Lac1 in the luminal region is important for the enzymatic activity of the complex.

Since the TM7/8 loop of Lac1 plays a key role in defining the acyl chain binding tunnel, we suspected that mutations in Lip1, responsible for the binding with TM7/8 loop of Lac1, may directly perturb the acyl chain binding tunnel (Fig 4C), leading to the greatly reduced catalytic activity of the mutants (Fig 4D). To corroborate this hypothesis, we determined the cryo-EM structure of the Lac1-Lip1^{S74F} mutant at an overall resolution of 3.85 Å (Appendix Fig S5A–F). By comparing the structure of the Lac1-Lip1^{S74F} heterodimer with that of the WT Lac1-Lip1 heterodimer, we observed that the Lip1^{S74F} mutation caused an evident conformational change in the TM7/8 loop of Lac1 (Fig 4E). More importantly, the C26 acyl chain binding tunnel within Lac1 observed in the WT complex collapsed in the Lip1^{S74F} mutant complex (Fig 4F), accomplished by some local conformational changes of residues lining the acyl chain binding tunnel (Fig 4G). Conformational changes in the residues lining the acyl chain binding tunnel, such as W371 and K293, which are distant from Lip1^{S74F}, could potentially be attributed to the subtle perturbation of the Lac1 structure resulting from the direct conformational change of the TM7/8 loop. The collapsed acyl chain binding tunnel presumably explains the abolished catalytic activity of the Lip1^{S74F} mutant complex (Fig 4D). Altogether, these studies suggest that the interaction of Lip1 and Lac1 in the luminal region is crucial for maintaining the proper acyl chain binding tunnel as well as the optimal activity of the complex.

A lateral opening on Lac1

In addition to a large cytosolic opening (Fig 1D), Lac1 also features a small lateral opening in the membrane-embedded region (Fig 5A). This lateral opening converges with the reaction chamber of Lac1 near the thioester bond of C26-CoA (Fig 5A), indicating that the

Figure 4. Interactions between Lac1 and Lip1.

- A Overall structure of a Lac1-Lip1 heterodimer. The two interaction interfaces between Lac1 and Lip1, namely the TM interaction interface and the luminal interaction interface, are highlighted with gray and red boxes, respectively.
- B, C Detailed views of the TM interaction interface between Lac1 and Lip1 (B) and the luminal interaction interface between Lac1 and Lip1 (C). All potential polar interactions are displayed by red dashed lines.
- D Functional characterization of Lip1 residues at the luminal interaction interface between Lac1 and Lip1 by CerS activity. Each data point is the average ± SEM of three independent experiments.
- E Structural superposition of the Lac1-Lip1^{WT} heterodimer (colored based on the subunits and domains) and the Lac1-Lip1^{S74F} heterodimer (colored light gray).
- F Collapse of the C26 acyl chain binding tunnel within Lac1 in the Lac1-Lip1^{S74F} mutant structure.
- G Local conformational changes of residues lining the C26-CoA binding site in the Lac1-Lip1^{S74F} mutant structure.

Source data are available online for this figure.

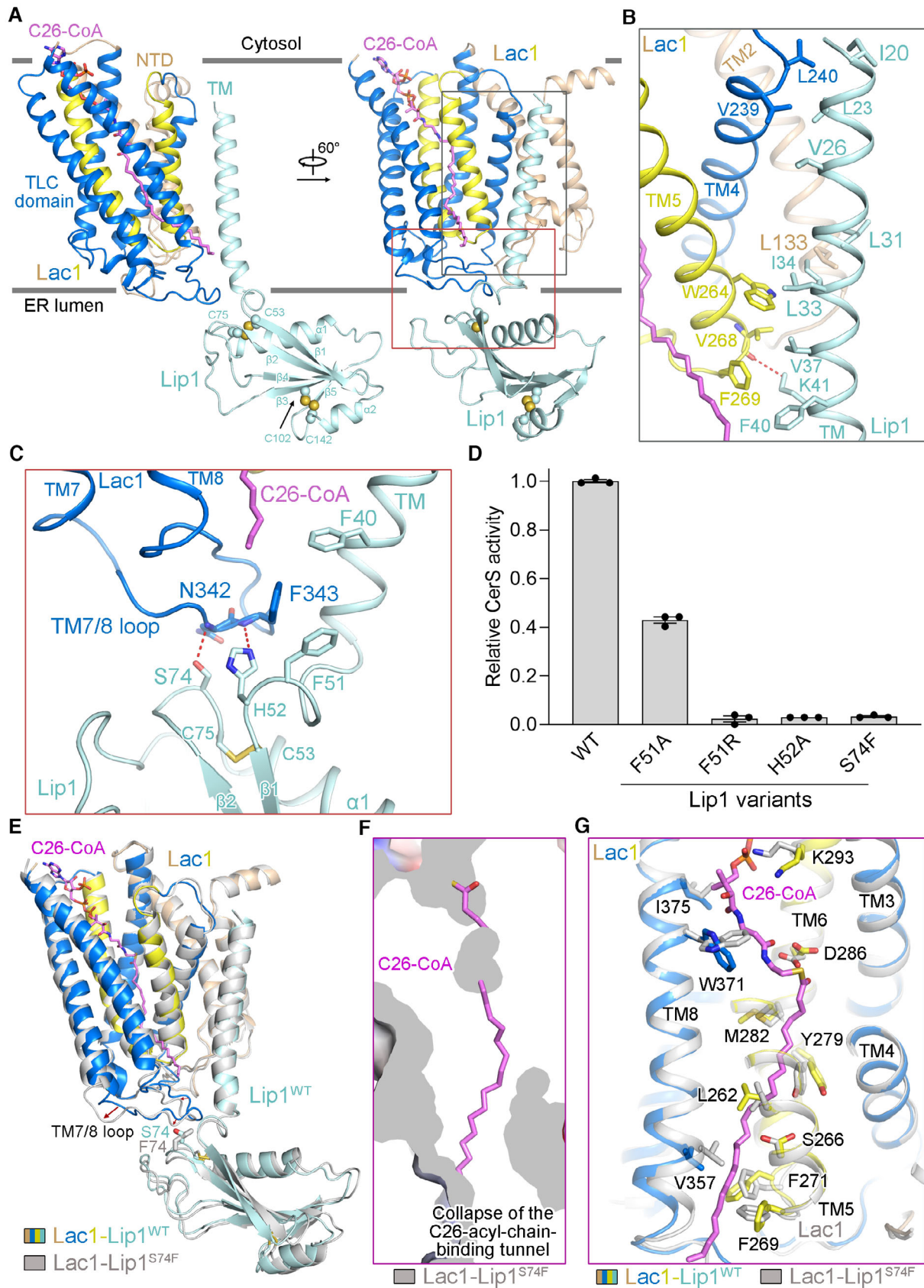


Figure 4.

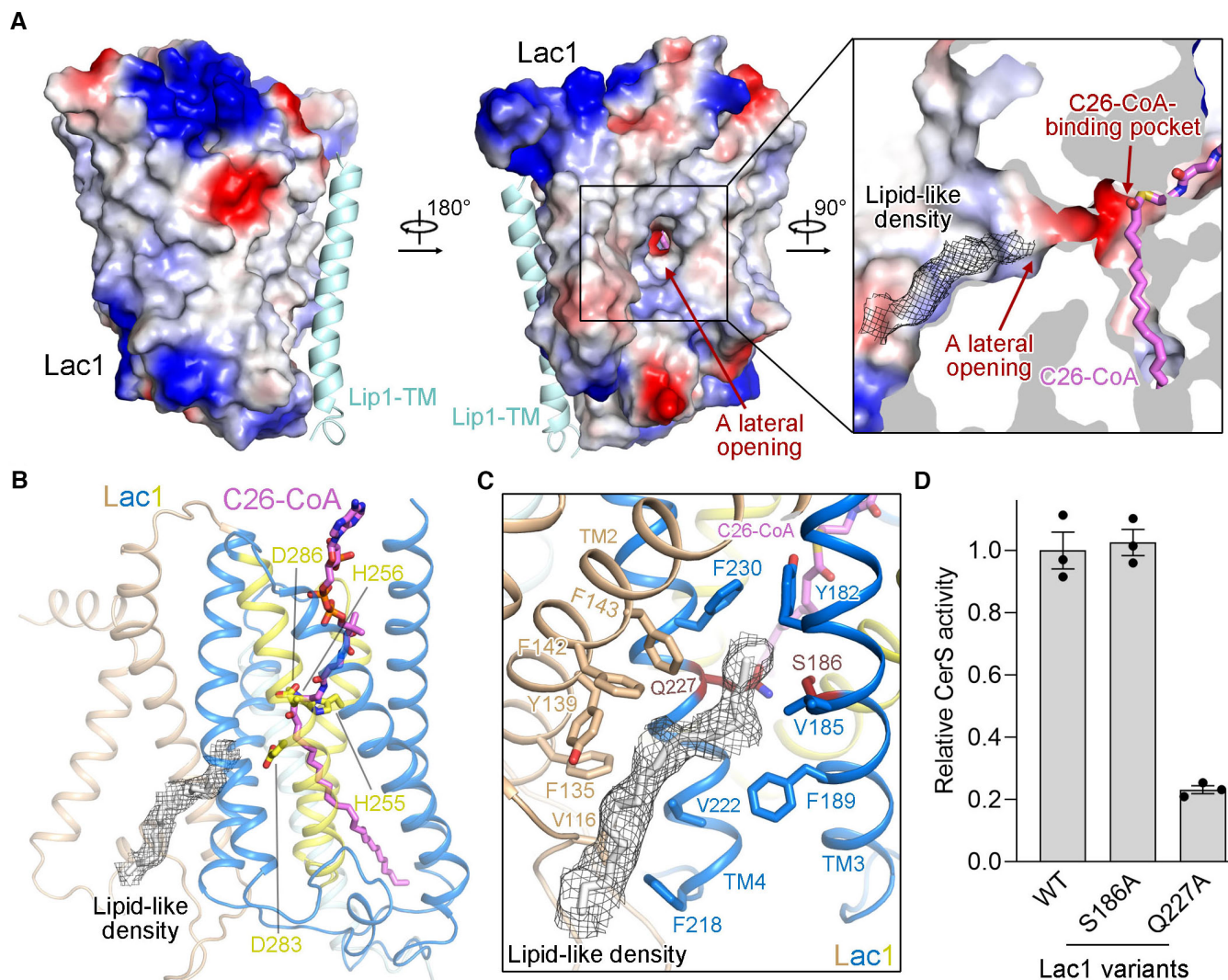


Figure 5. A lateral opening on Lac1.

A Detailed views of the lateral opening on Lac1.

B A lipid-like density stretches over the lateral opening and approaches the predicted catalytic sites. For visualization and clarification, an acyl chain was modeled into the lipid-like density.

C While the residues surrounding the lipid-like density are predominantly hydrophobic, two polar residues, Ser186 and Gln227, are located near the entrance of the lateral opening.

D CerS activity of the lateral-opening mutants. Each data point is the average \pm SEM of three independent experiments.

Source data are available online for this figure.

lateral opening could potentially serve as an entry site for the sphingoid base substrate. Consistent with this possibility, a lipid-like density was observed close to the lateral opening (Fig 5A). The lipid-like density stretches over the lateral opening and approaches the predicted catalytic sites (Fig 5B). The residues surrounding the lipid-like density are predominantly hydrophobic, but two polar residues, Ser186 and Gln227, are located in proximity to the entrance of the lateral opening (Fig 5C). Taken together, these structural observations support the hypothesis that the lateral opening on Lac1 may allow for the entrance of the sphingoid base substrate, with polar residues Ser186 and/or Gln227 potentially assisting in coordinating the polar head of the sphingoid base.

Mutating Ser186 to alanine did not affect the enzymatic activity of the complex, whereas mutating Gln227 to alanine greatly reduced the enzymatic activity of the complex to only about 20% of that of the WT complex (Fig 5D, Appendix Fig S4D). These results suggest that Gln227 is important for the catalytic activity of the complex, possibly due to its role in sphingoid base binding.

Discussion

The structure of the yeast CerS in complex with C26-CoA substrate presented here not only reveals that the holoenzyme is a dimer of

heterodimers but also elucidates the structural basis of C26-CoA binding. The structural observation, coupled with structure-guided mutational analysis, clarifies the use of a conserved hydrophilic reaction chamber in the ER membrane for catalysis. The C26-CoA thioester bond is located near the predicted catalytic His and Asp residues. The Lip1 subunit interacts with Lac1, fulfilling a crucial role in preserving a proper acyl chain binding tunnel and likely contributing to acyl chain binding. These findings shed light on the molecular mechanism underlying the stimulating effect of Lip1 on the catalytic activity of the complex. A lateral opening was revealed on Lac1 for the potential entrance of the sphingoid base substrate. These results provide a basis for understanding the catalytic mechanism of the CerS enzymes.

Based on our study, we proposed a working model for yeast CerS-catalyzed ceramide formation (Fig EV4A and B). The C26-CoA substrate enters the reaction chamber of Lac1-Lip1 heterodimer probably from the cytosolic side of the membrane leaflet. The CoA moiety of C26-CoA is located in the hydrophilic chamber, while the acyl-chain moiety lies in the hydrophobic tunnel (Fig EV4A, left). The sphingoid base substrate might approach the reaction chamber through a lateral opening on Lac1 (Fig EV4A, left). The sphingosine N-acyltransferase reaction for ceramide synthesis occurs through a proposed one-step catalytic mechanism (Fig EV4B), similar to that for Hedgehog (Hh) acyltransferase (HHAT), which accounts for the N-palmitoylation of Hh proteins (Jiang et al, 2021). In the proposed catalytic mechanism, Asp283 or Asp286 of Lac1 functions as a general base to activate the amino group of sphingoid base for nucleophilic attack on the carbonyl carbon of C26-CoA, which is coordinated by His255 or His256 (Fig EV4B). After the catalytic reaction, the product of free CoA-SH is released to the cytosol, whereas the hydrophobic product ceramide diffuses into the membrane bilayer (Fig EV4A, right). Further studies, including the structure of CerS in a complex with a sphingoid base substrate and the structures in distinct catalytic states, are necessary to delineate the precise catalytic mechanism.

Due to the current unavailability of an experimental high-resolution structure of mammalian CerS, we utilized AlphaFold-predicted human CerS structures (hCerS1^{AF}-hCerS6^{AF}) (Jumper et al, 2021) as substitutes to compare the structure–function relationship between mammalian CerS and yeast CerS (Fig EV5A and B). When hCerS5^{AF} was superimposed on the Lac1-Lip1 heterodimer, it was observed that the N-terminal region preceding TM1 of hCerS5^{AF}, which forms three short luminal helices (LH1-LH3) near the luminal side of the membrane, experienced severe clashes with the TM of Lip1 (Fig EV5B). These clashes could potentially provide an explanation for the absence of Lip1 homologs in mammals. Given the high conservation of both the hydrophilic reaction chamber (Fig 2C) and the upper portion of the acyl-chain binding tunnel (Fig 3E) among yeast and human CerS homologs, it is probable that human CerS homologs employ the same reaction chamber and tunnel as the Lac1-Lip1 complex to coordinate acyl-CoA substrates. However, the residues lining the lower portion of the acyl-chain binding tunnel do not exhibit conservation in yeast and human CerS homologs (Fig 3E), suggesting that these variable regions present in human CerS homologs might have a role in accommodating substrates with different acyl-chain lengths. Supporting this speculation, an 11-residue region within hCerS5^{AF} (referred to as acyl-CoA selective region in Figs EV1 and EV5A), belonging to these variable

regions, has been proposed to determine the acyl-CoA selectivity in mammalian CerS (Tidhar et al, 2018). Further structural and biochemical studies are needed to fully uncover the mechanism of acyl-CoA substrate selectivity in human CerS homologs.

The Lac1-Lip1 complex structure shows that the homo-dimeric organization of the Lac1-Lip1 holoenzyme is mediated only by the Lip1 subunit, while no interaction was found between the two Lac1 subunits. Mammalian CerS (except CerS1) have been shown to form both homo- and hetero-dimers via a conserved C-terminal DxRSDxE motif, and mammalian CerS activity can be modulated by homo- and hetero-dimerization (Laviad et al, 2012; Kim et al, 2022). This conserved dimerization motif is also present in yeast Lac1 and Lag1 (Fig EV1). This motif is not resolved in our structure, suggesting its intrinsic flexibility in the current structure. Interestingly, in our SEC experiments for large-scale purification of the Lac1-Lip1 complex, we often observed a larger but less abundant Lac1-Lip1 complex prior to the 2:2 Lac1-Lip1 complex peak (Appendix Fig S6A). Cryo-EM analysis of the larger Lac1-Lip1 complex revealed particles bigger than the 2:2 Lac1-Lip1 complex (Appendix Fig S6B). We could clearly identify two Lip1 dimers from the larger particles in the representative 2D averages (Appendix Fig S6B). The size and shape of the larger Lac1-Lip1 complex are consistent with a 4:4 Lac1-Lip1 complex, which is formed by two copies of 2:2 Lac1-Lip1 complexes through a dimerization interface mediated by Lac1 (Appendix Fig S6C). However, the larger Lac1-Lip1 complex appears to be highly heterogeneous in the cryo-EM samples (Appendix Fig S6B), hindering 3D reconstruction of the 4:4 Lac1-Lip1 complex. Further investigations are needed to determine the Lac1-mediated dimer interface and whether this interface regulates yeast CerS activity, as it will have important implications for understanding the molecular mechanisms by which mammalian CerS is regulated by dimerization.

Apart from the previously reported post-translational regulation of mammalian CerS via dimerization, both mammalian and yeast CerS have been revealed to be regulated via phosphorylation (Muir et al, 2014; Fresques et al, 2015; Sassa et al, 2016). Since the phosphorylation sequences at the N- and C-termini of Lac1 (Ser23/Ser24 and Ser393/Ser395/Ser397) are highly flexible in the resolved structures, further exploration is required to ascertain the molecular mechanism by which phosphorylation regulates CerS activity. Despite many remaining questions, the results presented in this study offer critical insights into the structure and mechanism of eukaryotic CerSs. These findings are considered important for understanding CerS biology and are expected to facilitate the rational design of CerS modulators for the treatment of metabolic diseases and cancers in the future.

Materials and Methods

Protein expression and purification

The full-length cDNA sequences of yeast Lac1 (Uniprot: P28496), Lag1 (Uniprot: P38703), and Lip1 (Uniprot: Q03579) were codon-optimized and individually subcloned into the pCAG vector fused with a Flag-tag or without a tag. All variants were generated with a standard two-step PCR-based strategy. The Flag-tag was added at the C-termini of Lac1, Lag1, and their variants, or the N-termini of

Lip1 and its variants. The Lac1-Lip1 complexes bearing Lac1 mutations were purified by the C-terminal Flag-tagged Lac1, while the Lac1-Lip1 complexes with Lip1 mutations were purified by the N-terminal Flag-tagged Lip1. HEK 293F suspension cells (Invitrogen) were grown in SMM 293T-II medium (Sino Biological Inc.) at 37°C, supplied with 5% CO₂ in a shaker. The cells were transiently transfected with one or two expression plasmids and polyethyleneimine (PEI) (Yeasen) at a cell density of around 2.5×10^6 cells per ml. About 1.5 mg of expression plasmids were preincubated with 4.5 mg PEI in 50 ml fresh medium for 15–30 min at room temperature before being applied to 1 liter of cell culture. After 12 h of infection, 10 mM sodium butyrate was added to boost protein expression for another 48 h. The cells were harvested by centrifugation at 4,000 g for 10 min. The cell pellets were flash-frozen in liquid nitrogen and stored at –80°C.

All protein purification steps were performed at 4°C. Cell pellets were resuspended in lysis buffer (25 mM HEPES pH 7.0, 150 mM NaCl) supplemented with a protease inhibitor cocktail (Amresco). The cell membranes were solubilized with 1% (w/v) GDN (Anatrace) at 4°C for 2 h. After centrifugation at 37,000 g for 1 h, the supernatant was collected and loaded onto anti-Flag G1 affinity resin (GenScript), rinsed with the wash buffer (W buffer) (25 mM HEPES pH 7.0, 150 mM NaCl, and 0.01% GDN). The resin was washed with 20 column volumes of W buffer before being eluted with W buffer plus Flag peptide (200 µg/ml). The protein was further purified by size-exclusion chromatography (SEC) using a Superose 6 Increase 10/300 GL column (GE Healthcare) equilibrated with W buffer. The peak fractions were pooled and concentrated for subsequent cryo-EM sample preparation. The protein for biochemical studies was purified similarly, except that the detergent used to solubilize the membrane was replaced by 1% (w/v) LMNG (Anatrace) and 0.2% (w/v) CHS (Anatrace).

In vitro CerS activity assay

A continuous spectrophotometric assay (Li *et al.*, 2021; Liu *et al.*, 2023; Xie *et al.*, 2023) was used to monitor the ceramide synthase activity of the purified protein by measuring the release of CoA-SH from acyl-CoA substrates. The sulfhydryl (-SH) group of CoA-SH reacts with 5,5'-dithiobis-2-nitrobenzoic acid (DTNB) to produce the yellow-colored TNB (5-thio-2-nitrobenzoic acid) with maximum absorbance at 412 nm. A standard curve with CoA-SH concentrations varying between 10 and 250 µM was produced. The assays were performed on a 50-µl scale at 37°C in 96-well plates with a BioTek plate reader. Absorbance at 412 nm was recorded for 1 h upon reaction initiation. A typical reaction mixture contained 0.3 µM yeast CerS protein complex, 0.4 mM DTNB, 100 µM DHS, 100 µM acyl-CoA, and 10% (v/v) DMSO in W buffer. To measure the curve of CerS activity versus various concentrations of C26-CoA, the DHS concentration was retained at 100 µM. To measure the curve of CerS activity versus various concentrations of DHS, the C26-CoA concentration was kept at 100 µM. The CerS activity was calculated from the raw data that stays in the linear range and determined according to the CoA-SH standard curve. The statistical analysis was performed with GraphPad Prism 8. For all dot-plot graphs and curves, each data point is the average of three independent experiments, and error bars represent SEM.

Sample preparation and cryo-EM data collection

For the cryo-EM sample preparation of the C26-CoA-bound Lac1-Lip1 complex, a final concentration of 30 µM C26-CoA was added into the elution buffer during protein purification, and 0.5 mM C26-CoA was incubated with 20 mg/ml Lac1-Lip1 complex at 4°C for 30 min before grid preparation. The Quantifoil Cu R1.2/1.3300 mesh grids were glow-discharged at 15 mA for 45 s in a PELCO easiGlow device before use. Aliquots of 3 µl purified protein were applied to the glow-discharged grids. After blotting for 4.5 s at 8°C with 100% humidity, the grids were flash-frozen in liquid ethane and cooled by liquid nitrogen using Vitrobot (Mark IV, Thermo Fisher Scientific). The sample preparation for the Lac1-Lip1^{S74F} complex was performed similarly without adding extra C26-CoA. The datasets were collected with EPU automatically on a 300 kV Titan Krios microscope equipped with a GIF Quantum energy filter (Gatan) with a slit width of 20 eV and a K3 Summit direct electron detector (Gatan). All movie stacks were recorded at a nominal magnification of $\times 81,000$ with defocus values from –2.0 to –1.0 µm. Each stack was exposed in super-resolution mode for 2.3 s in 32 frames with a total dose of $50 \text{ e}^-/\text{Å}^2$.

Cryo-EM data processing

Data processing procedures were summarized in flow charts in the Appendix Figs S1C and S5C. For the C26-CoA-bound Lac1-Lip1 complex and the Lac1-Lip1^{S74F} complex, a total of 5,059 and 2,721 micrographs were collected, respectively. The stacks were motion corrected with dose weighting using MotionCor2 (Zheng *et al.*, 2017), and binned twofold, resulting in a pixel size of 1.072 Å. The defocus values were estimated by Gctf (Zhang, 2016). A total of 5,112,832 and 2,355,239 particles were automatically picked from the two datasets in Relion 3.0 (Zivanov *et al.*, 2018), respectively. All the following data processing procedures were performed in CryoSPARC (Punjani *et al.*, 2017). A total of 862,488 and 626,235 particles were selected from the 2D classifications for the C26-CoA-bound Lac1-Lip1 complex and the Lac1-Lip1^{S74F} complex, respectively. After two rounds of multiclass ab-initio reconstruction, heterogeneous refinement, and non-uniform refinement, 355,520 and 213,962 particles with good structural features were chosen, respectively. A further round of resolution-gradient classification, non-uniform refinement, and local refinement with C2 symmetry yielded reconstructions with overall resolutions of 3.09 and 3.85 Å with 179,070 and 93,964 particles for the C26-CoA-bound Lac1-Lip1 complex and the Lac1-Lip1^{S74F} complex, respectively. Resolutions were estimated by the gold-standard Fourier shell correlation 0.143 criterion (Rosenthal & Henderson, 2003) with high-resolution noise substitution (Chen *et al.*, 2013).

Model building and refinement

The Lac1 and Lip1 models predicted from AlphaFold were used as the initial models for C26-CoA-bound Lac1-Lip1 model building. The predicted models were docked into the map using UCSF Chimera (Pettersen *et al.*, 2004). Each residue was manually adjusted in Coot (Emsley *et al.*, 2010). Structure refinements were carried out by Phenix (Adams *et al.*, 2010) in real space with secondary structure and geometry restraints. The C26-CoA-bound Lac1-Lip1

structure was used as the initial model for the Lac1-Lip1^{S74F} model building. All the structural models were validated using Phenix and MolProbity (Williams *et al*, 2018). The refinement and validation statistics were summarized in Appendix Table S1. All structural figures were prepared using PyMol (DeLano, 2002) or Chimera.

Data availability

The EM density maps generated in this study have been deposited in the EMDB under accession codes EMD-35862 (<https://www.ebi.ac.uk/emdb/EMD-35862>) for C26-CoA-bound Lac1-Lip1 complex and EMD-35863 (<https://www.ebi.ac.uk/emdb/EMD-35863>) for Lac1-Lip1^{S74F} complex. The atomic coordinates have been deposited in the PDB under the accession codes 8IZD (<https://www.rcsb.org/structure/8IZD>) for C26-CoA-bound Lac1-Lip1 complex and 8IZF (<https://www.rcsb.org/structure/8IZF>) for Lac1-Lip1^{S74F} complex. Source data are provided with the manuscript.

Expanded View for this article is available [online](#).

Acknowledgements

We thank the Cryo-EM Facility of the Southern University of Science and Technology (SUSTech) for providing the facility support. We are grateful to Ma X., Gao Y., and all the other staffs in the SUSTech cryo-EM center for their technical support on data collection. This work was supported by the National Natural Science Foundation of China (32122043 and 92057101 to XG), the Guangdong Basic and Applied Basic Research Foundation (2019B151502047 to XG), and the Shenzhen Science and Technology Program (RCYX20200714114522081 and 20220815111002002 to XG).

Author contributions

Xin Gong: Conceptualization; formal analysis; supervision; funding acquisition; writing – original draft; writing – review and editing. **Tian Xie:** Data curation; formal analysis; writing – review and editing. **Qi Fang:** Data curation; formal analysis. **Zike Zhang:** Data curation. **Yanfei Wang:** Data curation. **Feitong Dong:** Data curation.

Disclosure and competing interests statement

The authors declare that they have no conflict of interest.

References

- Adams PD, Afonine PV, Bunkoczi G, Chen VB, Davis IW, Echols N, Headd JJ, Hung LW, Kapral GJ, Grosse-Kunstleve RW *et al* (2010) PHENIX: a comprehensive Python-based system for macromolecular structure solution. *Acta Crystallogr D Biol Crystallogr* 66: 213–221
- Barz WP, Walter P (1999) Two endoplasmic reticulum (ER) membrane proteins that facilitate ER-to-Golgi transport of glycosylphosphatidylinositol-anchored proteins. *Mol Biol Cell* 10: 1043–1059
- Brachtendorf S, El-Hindi K, Grösch S (2019) Ceramide synthases in cancer therapy and chemoresistance. *Prog Lipid Res* 74: 160–185
- Chaurasia B, Summers SA (2015) Ceramides - lipotoxic inducers of metabolic disorders. *Trends Endocrinol Metab* 26: 538–550
- Chaurasia B, Summers SA (2021) Ceramides in metabolism: key lipotoxic players. *Annu Rev Physiol* 83: 303–330
- Chen SX, McMullan G, Faruqi AR, Murshudov GN, Short JM, Scheres SHW, Henderson R (2013) High-resolution noise substitution to measure overfitting and validate resolution in 3D structure determination by single particle electron cryomicroscopy. *Ultramicroscopy* 135: 24–35
- Choi RH, Tatum SM, Symons JD, Summers SA, Holland WL (2021) Ceramides and other sphingolipids as drivers of cardiovascular disease. *Nat Rev Cardiol* 18: 701–711
- DeLano WL (2002) The PyMOL molecular graphics system on world wide web. <http://www.pymol.org>
- Emsley P, Lohkamp B, Scott WG, Cowtan K (2010) Features and development of Coot. *Acta Crystallogr D Biol Crystallogr* 66: 486–501
- Fresques T, Niles B, Aronova S, Mogri H, Rakhshandehroo T, Powers T (2015) Regulation of ceramide synthase by casein kinase 2-dependent phosphorylation in *Saccharomyces cerevisiae*. *J Biol Chem* 290: 1395–1403
- Gault CR, Obeid LM, Hannun YA (2010) An overview of sphingolipid metabolism: from synthesis to breakdown. *Adv Exp Med Biol* 688: 1–23
- Guillas I, Kirchman PA, Chuard R, Pfeifferli M, Jiang JC, Jazwinski SM, Conzelmann A (2001) C26-CoA-dependent ceramide synthesis of *Saccharomyces cerevisiae* is operated by Lag1p and Lac1p. *EMBO J* 20: 2655–2665
- Guillas I, Jiang JC, Vionnet C, Roubaty C, Uldry D, Chuard R, Wang J, Jazwinski SM, Conzelmann A (2003) Human homologues of LAG1 reconstitute Acyl-CoA-dependent ceramide synthesis in yeast. *J Biol Chem* 278: 37083–37091
- Hannun YA, Obeid LM (2008) Principles of bioactive lipid signalling: lessons from sphingolipids. *Nat Rev Mol Cell Biol* 9: 139–150
- Hannun YA, Obeid LM (2011) Many ceramides. *J Biol Chem* 286: 27855–27862
- Hannun YA, Obeid LM (2018) Sphingolipids and their metabolism in physiology and disease. *Nat Rev Mol Cell Biol* 19: 175–191
- Harrison PJ, Dunn TM, Campopiano DJ (2018) Sphingolipid biosynthesis in man and microbes. *Nat Prod Rep* 35: 921–954
- Havulinna AS, Sysi-Aho M, Hilvo M, Kauhanen D, Hurme R, Ekroos K, Salomaa V, Laaksonen R (2016) Circulating ceramides predict cardiovascular outcomes in the population-based FINRISK 2002 cohort. *Arterioscler Thromb Vasc Biol* 36: 2424–2430
- Hilvo M, Meikle PJ, Pedersen ER, Tell GS, Dhar I, Brenner H, Schöttker B, Lääperi M, Kauhanen D, Koistinen KM *et al* (2020) Development and validation of a ceramide- and phospholipid-based cardiovascular risk estimation score for coronary artery disease patients. *Eur Heart J* 41: 371–380
- Hla T, Dannenberg AJ (2012) Sphingolipid signaling in metabolic disorders. *Cell Metab* 16: 420–434
- Holm L (2022) Dali server: structural unification of protein families. *Nucleic Acids Res* 50: W210–W215
- Jiang JC, Kirchman PA, Zagulski M, Hunt J, Jazwinski SM (1998) Homologs of the yeast longevity gene LAG1 in *Caenorhabditis elegans* and human. *Genome Res* 8: 1259–1272
- Jiang Y, Benz TL, Long SB (2021) Substrate and product complexes reveal mechanisms of Hedgehog acylation by HHAT. *Science* 372: 1215–1219
- Jumper J, Evans R, Pritzel A, Green T, Figurnov M, Ronneberger O, Tunyasuvunakool K, Bates R, Židek A, Potapenko A *et al* (2021) Highly accurate protein structure prediction with AlphaFold. *Nature* 596: 583–589
- Kageyama-Yahara N, Riezman H (2006) Transmembrane topology of ceramide synthase in yeast. *Biochem J* 398: 585–593
- Karjalainen JP, Mononen N, Hutri-Kähönen N, Lehtimäki M, Hilvo M, Kauhanen D, Juonala M, Viikari J, Kähönen M, Raitakari O *et al* (2019) New evidence from plasma ceramides links apoE polymorphism to greater risk of coronary artery disease in Finnish adults. *J Lipid Res* 60: 1622–1629
- Kim JL, Ben-Dor S, Rosenfeld-Gur E, Futerman AH (2022) A novel C-terminal DxRSDxE motif in ceramide synthases involved in dimer formation. *J Biol Chem* 298: 101517

- Laaksonen R, Ekroos K, Sysi-Aho M, Hilvo M, Vihervaara T, Kauhanen D, Suoniemi M, Hurme R, März W, Scharnagl H *et al* (2016) Plasma ceramides predict cardiovascular death in patients with stable coronary artery disease and acute coronary syndromes beyond LDL-cholesterol. *Eur Heart J* 37: 1967–1976
- Laviad EL, Albee L, Pankova-Kholmyansky I, Epstein S, Park H, Merrill AH Jr, Futerman AH (2008) Characterization of ceramide synthase 2: tissue distribution, substrate specificity, and inhibition by sphingosine 1-phosphate. *J Biol Chem* 283: 5677–5684
- Laviad EL, Kelly S, Merrill AH Jr, Futerman AH (2012) Modulation of ceramide synthase activity via dimerization. *J Biol Chem* 287: 21025–21033
- Lemaitre RN, Yu C, Hoofnagle A, Hari N, Jensen PN, Fretts AM, Umans JG, Howard BV, Sitlani CM, Siscovick DS *et al* (2018) Circulating sphingolipids, insulin, HOMA-IR, and HOMA-B: the Strong Heart Family Study. *Diabetes* 67: 1663–1672
- Levy M, Futerman AH (2010) Mammalian ceramide synthases. *IUBMB Life* 62: 347–356
- Li S, Xie T, Liu P, Wang L, Gong X (2021) Structural insights into the assembly and substrate selectivity of human SPT-ORMDL3 complex. *Nat Struct Mol Biol* 28: 249–257
- Liu P, Xie T, Wu X, Han G, Gupta SD, Zhang Z, Yue J, Dong F, Gable K, Niranjankumari S *et al* (2023) Mechanism of sphingolipid homeostasis revealed by structural analysis of *Arabidopsis* SPT-ORM1 complex. *Sci Adv* 9: eadg0728
- Mantovani A, Bonapace S, Lunardi G, Salgarello M, Dugo C, Gori S, Barbieri E, Verlato G, Laaksonen R, Byrne CD *et al* (2018) Association of plasma ceramides with myocardial perfusion in patients with coronary artery disease undergoing stress myocardial perfusion scintigraphy. *Arterioscler Thromb Vasc Biol* 38: 2854–2861
- Mantovani A, Bonapace S, Lunardi G, Canali G, Dugo C, Vinco G, Calabria S, Barbieri E, Laaksonen R, Bonnet F *et al* (2020) Associations between specific plasma ceramides and severity of coronary-artery stenosis assessed by coronary angiography. *Diabetes Metab* 46: 150–157
- Mizutani Y, Kihara A, Igarashi Y (2005) Mammalian Lass6 and its related family members regulate synthesis of specific ceramides. *Biochem J* 390: 263–271
- Mizutani Y, Kihara A, Igarashi Y (2006) LASS3 (longevity assurance homologue 3) is a mainly testis-specific (dihydro)ceramide synthase with relatively broad substrate specificity. *Biochem J* 398: 531–538
- Muir A, Ramachandran S, Roelants FM, Timmons G, Thorner J (2014) TORC2-dependent protein kinase Ypk1 phosphorylates ceramide synthase to stimulate synthesis of complex sphingolipids. *Elife* 3: e03779
- Mullen TD, Hannun YA, Obeid LM (2012) Ceramide synthases at the centre of sphingolipid metabolism and biology. *Biochem J* 441: 789–802
- Park JW, Park WJ, Futerman AH (2014) Ceramide synthases as potential targets for therapeutic intervention in human diseases. *Biochim Biophys Acta* 1841: 671–681
- Pettersen EF, Goddard TD, Huang CC, Couch GS, Greenblatt DM, Meng EC, Ferrin TE (2004) UCSF Chimera—a visualization system for exploratory research and analysis. *J Comput Chem* 25: 1605–1612
- Pewzner-Jung Y, Ben-Dor S, Futerman AH (2006) When do Lass6 (longevity assurance genes) become CerS (ceramide synthases)? insights into the regulation of ceramide synthesis. *J Biol Chem* 281: 25001–25005
- Poss AM, Holland WL, Summers SA (2020a) Risky lipids: refining the ceramide score that measures cardiovascular health. *Eur Heart J* 41: 381–382
- Poss AM, Maschek JA, Cox JE, Hauner BJ, Hopkins PN, Hunt SC, Holland WL, Summers SA, Playdon MC (2020b) Machine learning reveals serum sphingolipids as cholesterol-independent biomarkers of coronary artery disease. *J Clin Invest* 130: 1363–1376
- Punjani A, Rubinstein JL, Fleet DJ, Brubaker MA (2017) cryoSPARC: algorithms for rapid unsupervised cryo-EM structure determination. *Nat Methods* 14: 290–296
- Raichur S (2020) Ceramide synthases are attractive drug targets for treating metabolic diseases. *Front Endocrinol* 11: 483
- Riebeling C, Allegood JC, Wang E, Merrill AH Jr, Futerman AH (2003) Two mammalian longevity assurance gene (LAG1) family members, trh1 and trh4, regulate dihydroceramide synthesis using different fatty acyl-CoA donors. *J Biol Chem* 278: 43452–43459
- Rosenthal PB, Henderson R (2003) Optimal determination of particle orientation, absolute hand, and contrast loss in single-particle electron cryomicroscopy. *J Mol Biol* 333: 721–745
- Sassa T, Hirayama T, Kihara A (2016) Enzyme activities of the ceramide synthases CERS2-6 are regulated by phosphorylation in the C-terminal region. *J Biol Chem* 291: 7477–7487
- Schorling S, Vallée B, Barz WP, Riezman H, Oesterheld D (2001) Lag1p and Lac1p are essential for the Acyl-CoA-dependent ceramide synthase reaction in *Saccharomyces cerevisiae*. *Mol Biol Cell* 12: 3417–3427
- Spassieva S, Seo JG, Jiang JC, Bielawski J, Alvarez-Vasquez F, Jazwinski SM, Hannun YA, Obeid LM (2006) Necessary role for the Lag1p motif in (dihydro)ceramide synthase activity. *J Biol Chem* 281: 33931–33938
- Summers SA (2018) Could ceramides become the new cholesterol? *Cell Metab* 27: 276–280
- Summers SA, Chaurasia B, Holland WL (2019) Metabolic messengers: ceramides. *Nat Metab* 1: 1051–1058
- Tidhar R, Ben-Dor S, Wang E, Kelly S, Merrill AH Jr, Futerman AH (2012) Acyl chain specificity of ceramide synthases is determined within a region of 150 residues in the Tram-Lag-CLN8 (TLC) domain. *J Biol Chem* 287: 3197–3206
- Tidhar R, Zelnik ID, Volpert G, Ben-Dor S, Kelly S, Merrill AH Jr, Futerman AH (2018) Eleven residues determine the acyl chain specificity of ceramide synthases. *J Biol Chem* 293: 9912–9921
- Turpin-Nolan SM, Brüning JC (2020) The role of ceramides in metabolic disorders: when size and localization matters. *Nat Rev Endocrinol* 16: 224–233
- Vallée B, Riezman H (2005) Lip1p: a novel subunit of acyl-CoA ceramide synthase. *EMBO J* 24: 730–741
- Venkataraman K, Riebeling C, Bodenec J, Riezman H, Allegood JC, Sullards MC, Merrill AH Jr, Futerman AH (2002) Upstream of growth and differentiation factor 1 (uog1), a mammalian homolog of the yeast longevity assurance gene 1 (LAG1), regulates N-stearoyl-sphinganine (C18-(dihydro)ceramide) synthesis in a fumonisins B1-independent manner in mammalian cells. *J Biol Chem* 277: 35642–35649
- Wang Y, Niu Y, Zhang Z, Gable K, Gupta SD, Somashekarappa N, Han G, Zhao H, Myasnikov AG, Kalathur RC *et al* (2021) Structural insights into the regulation of human serine palmitoyltransferase complexes. *Nat Struct Mol Biol* 28: 240–248
- Williams CJ, Headd JJ, Moriarty NW, Prisant MG, Videau LL, Deis LN, Verma V, Keedy DA, Hintze BJ, Chen VB *et al* (2018) MolProbity: more and better reference data for improved all-atom structure validation. *Protein Sci* 27: 293–315
- Winter E, Ponting CP (2002) TRAM, LAG1 and CLN8: members of a novel family of lipid-sensing domains? *Trends Biochem Sci* 27: 381–383
- Xie T, Liu P, Wu X, Dong F, Zhang Z, Yue J, Mahawar U, Farooq F, Vohra H, Fang Q *et al* (2023) Ceramide sensing by human SPT-ORMDL complex for establishing sphingolipid homeostasis. *Nat Commun* 14: 3475

- Yariv B, Yariv E, Kessel A, Masrati G, Chorin AB, Martz E, Mayrose I, Pupko T, Ben-Tal N (2023) Using evolutionary data to make sense of macromolecules with a “face-lifted” ConSurf. *Protein Sci* 32: e4582
- Zhang K (2016) Gctf: real-time CTF determination and correction. *J Struct Biol* 193: 1–12
- Zheng SQ, Palovcak E, Armache JP, Verba KA, Cheng Y, Agard DA (2017) MotionCor2: anisotropic correction of beam-induced motion for improved cryo-electron microscopy. *Nat Methods* 14: 331–332
- Zivanov J, Nakane T, Forsberg BO, Kimanius D, Hagen WJ, Lindahl E, Scheres SH (2018) New tools for automated high-resolution cryo-EM structure determination in RELION-3. *Elife* 7: e42166

Expanded View Figures

Figure EV1. Sequence alignments of yeast Lac1 and Lag1, and human CerS family members.

Secondary structural elements of yeast Lac1 are labeled above the sequence alignment. CH: cytosolic helix; TM: transmembrane helix; LH: luminal helix. The NTD is colored wheat. The TLC domain is colored marine with the Lag1p motif shown in yellow. The four red triangles indicate the predicted catalytic histidine and aspartate residues in the Lag1p motif. The Hox domains and acyl-CoA selective regions in human CerS are highlighted with wheat and dark pink boxes, respectively. The DxRSDxE dimerization motif is highlighted with a green box. The UniProt IDs for the aligned sequences are as follows: yLac1: P28496; yLag1: P38703; hCerS1: P27544; hCerS2: Q96G23; hCerS3: Q8IU89; hCerS4: Q9HA82; hCerS5: Q8N5B7; and hCerS6: Q6ZMG9. "y" for *Saccharomyces cerevisiae* (yeast) and "h" for *Homo sapiens* (human).

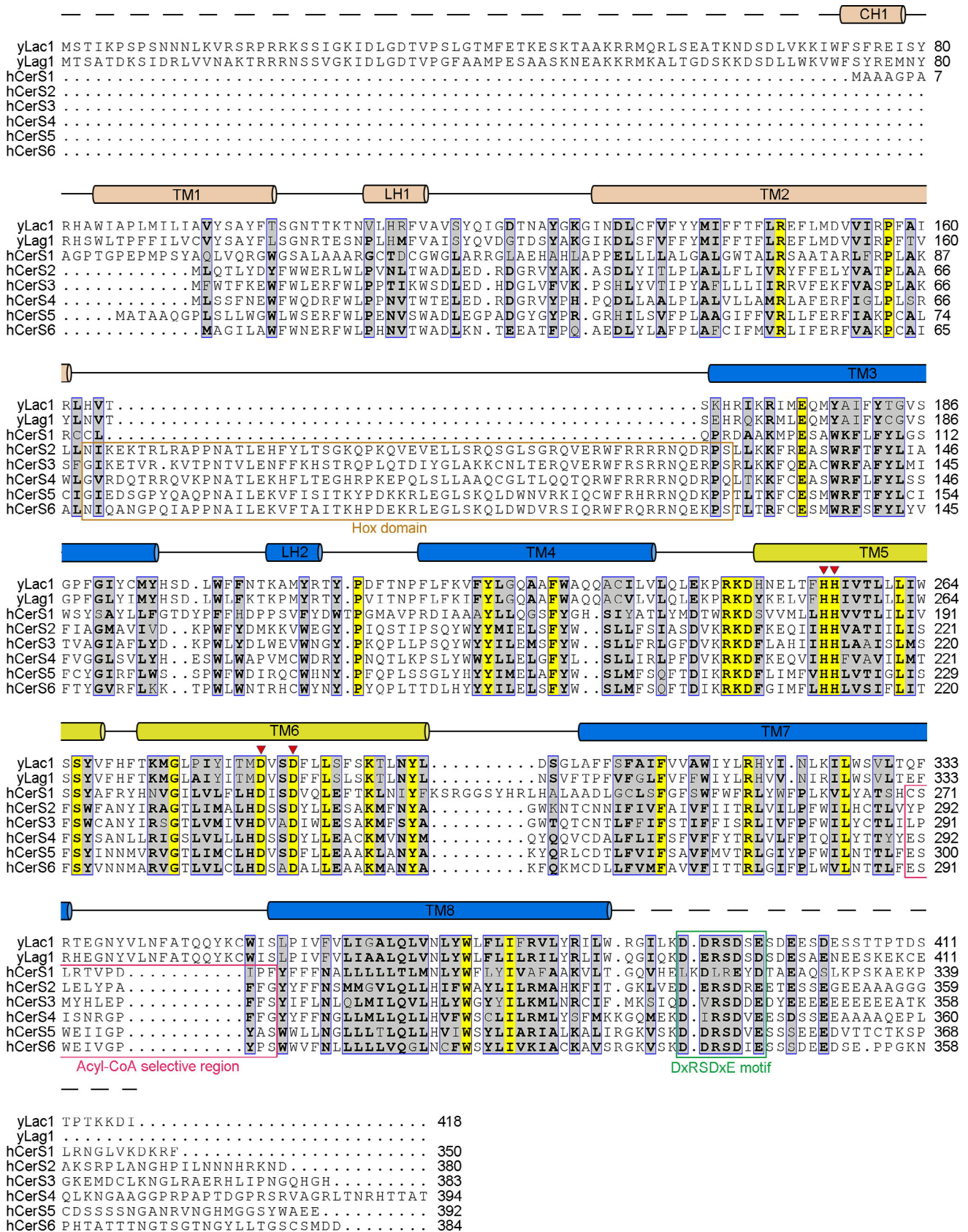


Figure EV1.

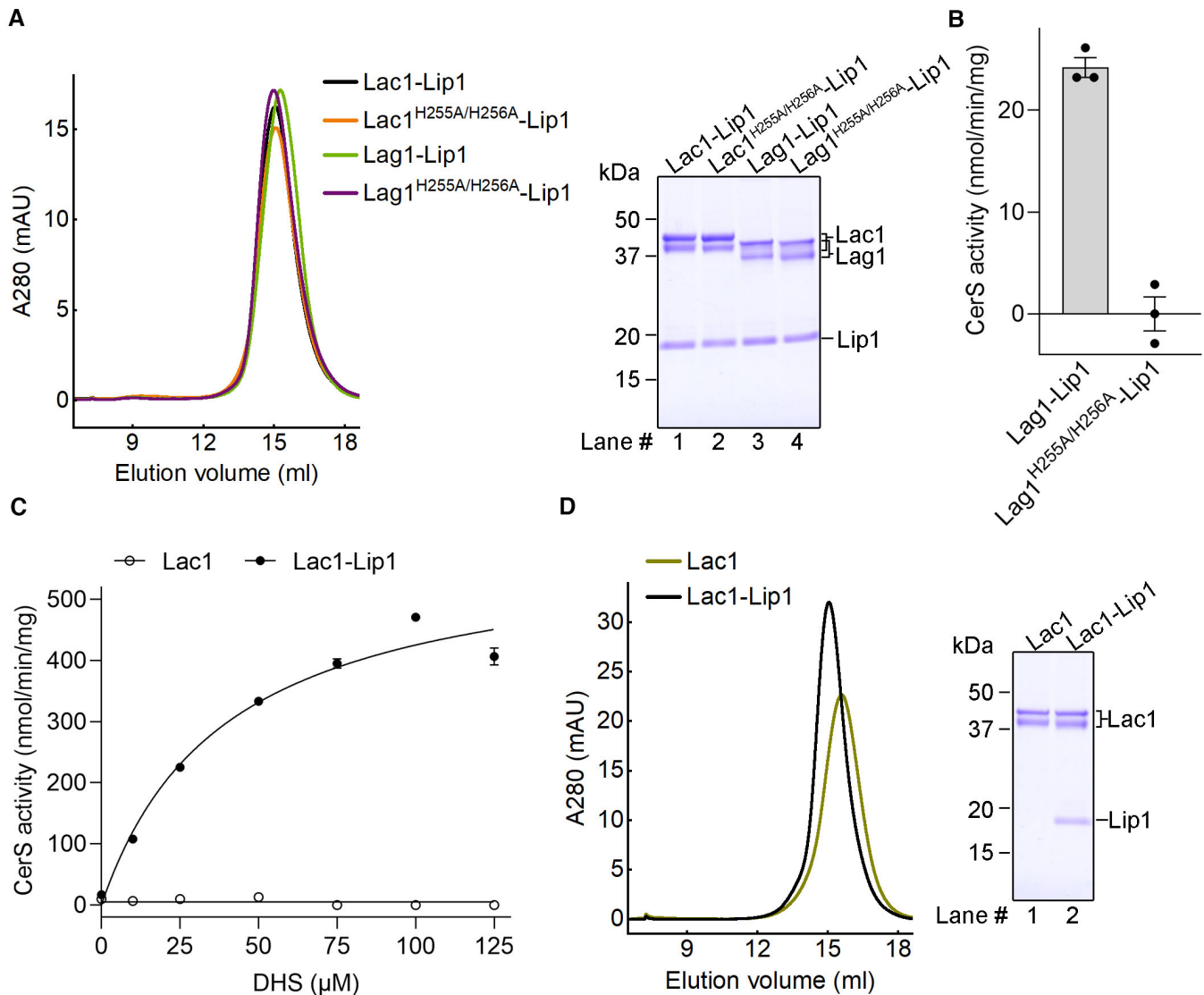


Figure EV2. Biochemical characterization of the Lac1-Lip1 and Lag1-Lip1 complexes.

- A Size exclusion chromatography (SEC) profiles and Coomassie blue-stained SDS-PAGE gel of the purified Lac1-Lip1 and Lag1-Lip1 complexes.
- B Enzymatic activity of the WT Lag1-Lip1 complex and the catalytic mutant Lag1^{H255A/H256A}-Lip1. Each data point is the average \pm SEM of three independent experiments.
- C CerS activity versus DHS concentration for the Lac1 alone protein and the Lac1-Lip1 complex. The activity curve of the Lac1-Lip1 complex follows a Michaelis-Menten equation with a K_m of $39.44 \pm 6.29 \mu\text{M}$ for DHS and a V_{max} of $593.3 \pm 34.5 \text{ nmol/min/mg}$. Each data point is the average \pm SEM of three independent experiments.
- D SEC profile and Coomassie blue-stained SDS-PAGE gel of the Lac1 alone protein and the Lac1-Lip1 complex.

Figure EV3. Features of Lip1 dimer.

- A Overall structure of Lip1 dimer.
- B Lip1 dimer interface.
- C SEC profiles and Coomassie blue-stained SDS-PAGE gel of the Lip1 cysteine mutants.
- D Normalized CerS activity of the Lip1 cysteine mutants. Each data point is the average \pm SEM of three independent experiments.
- E SEC profile and Coomassie blue-stained SDS-PAGE gel of the Lip1 dimer interface variant.
- F Normalized CerS activity of the Lip1 dimer interface variant. Each data point is the average \pm SEM of three independent experiments.

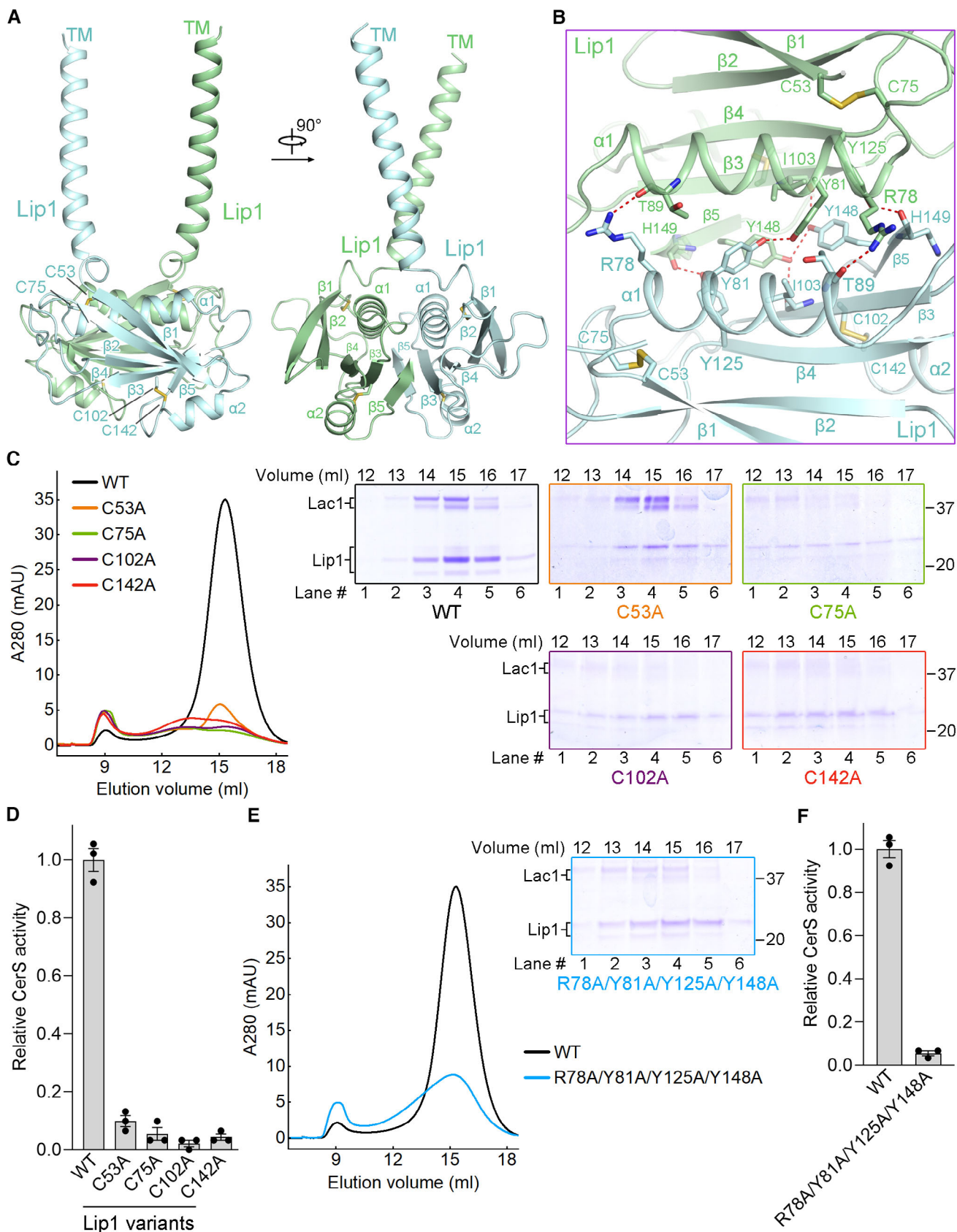


Figure EV3.

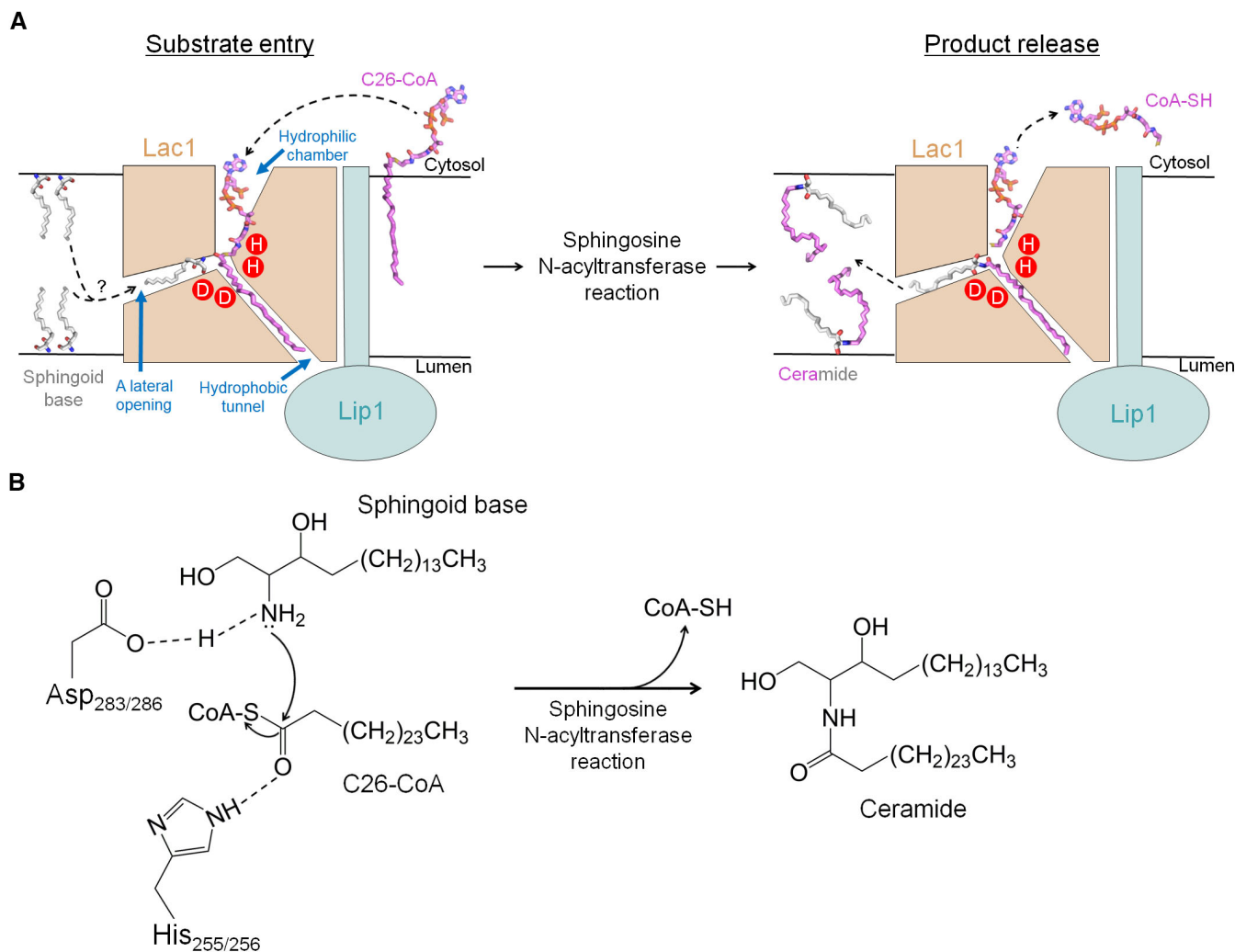


Figure EV4. Proposed working mechanism of yeast CerS.

- A A hypothetical model for yeast CerS-catalyzed ceramide formation. The C26-CoA substrate enters the reaction chamber within Lac1 probably through the cytosolic side of the membrane. The CoA moiety of C26-CoA is located in the hydrophilic reaction chamber, while the acyl-chain moiety is positioned in the hydrophobic tunnel. Once the sphingoid base substrate from either leaflet of the membrane enters a lateral opening on Lac1, it approaches the catalytic histidine and aspartate residues near the thioester bond of C26-CoA, preparing for the sphingosine N-acyltransferase reaction. After the reaction, the product of free CoA-SH is released to the cytosol, whereas the hydrophobic product ceramide is released to either leaflet of the membrane. For simplicity, only one Lac1-Lip1 heterodimer is illustrated.
- B Proposed catalytic mechanism. Asp283 or Asp286 of Lac1 functions as a general base to activate the amino group of the sphingoid base for nucleophilic attack on the carbonyl carbon of C26-CoA, which is coordinated by His255 or His256. The CerS-catalyzed acyl transfer reaction promotes the N-acylation of sphingoid base for ceramide production and releases free CoA-SH.

Figure EV5. Human CerS structural models predicted by AlphaFold.

- A The AlphaFold-predicted human CerS structures (hCerS1AF-hCerS6AF). The N-terminal regions and Hox domains of hCerSs are colored light gray. The TLC domains are colored green with the acyl-CoA selective regions highlighted in dark pink. The predicted catalytic histidine and aspartate residues in the Lag1p motifs are shown in sticks.
- B Structural superposition of the hCerS5AF (colored green) and the Lac1-Lip1 heterodimer (colored wheat and light cyan). The N-terminal region of hCerS5AF severely clashes with the TM of Lip1.

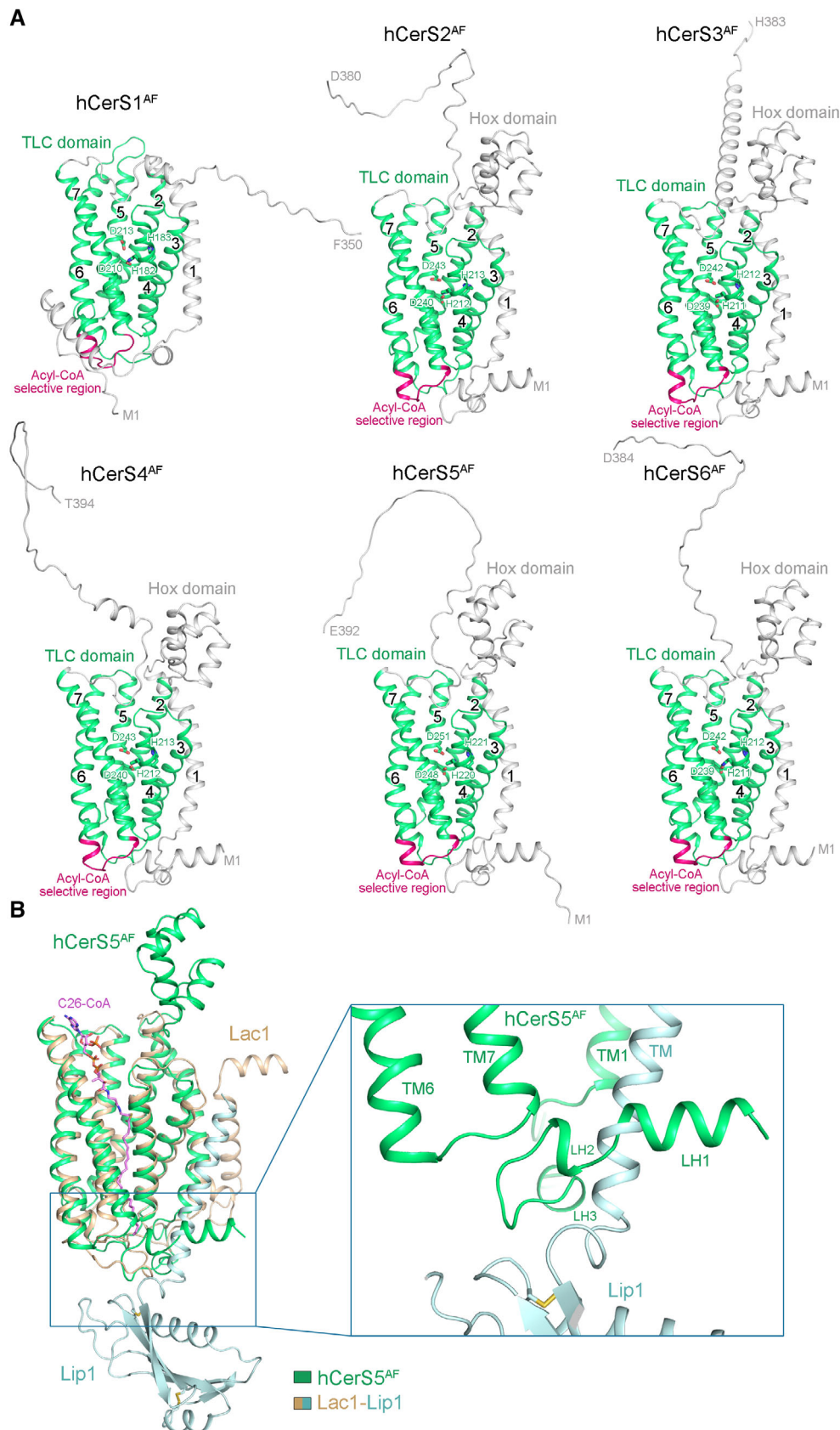


Figure EV5.

Appendix Figures and Tables

For the manuscript

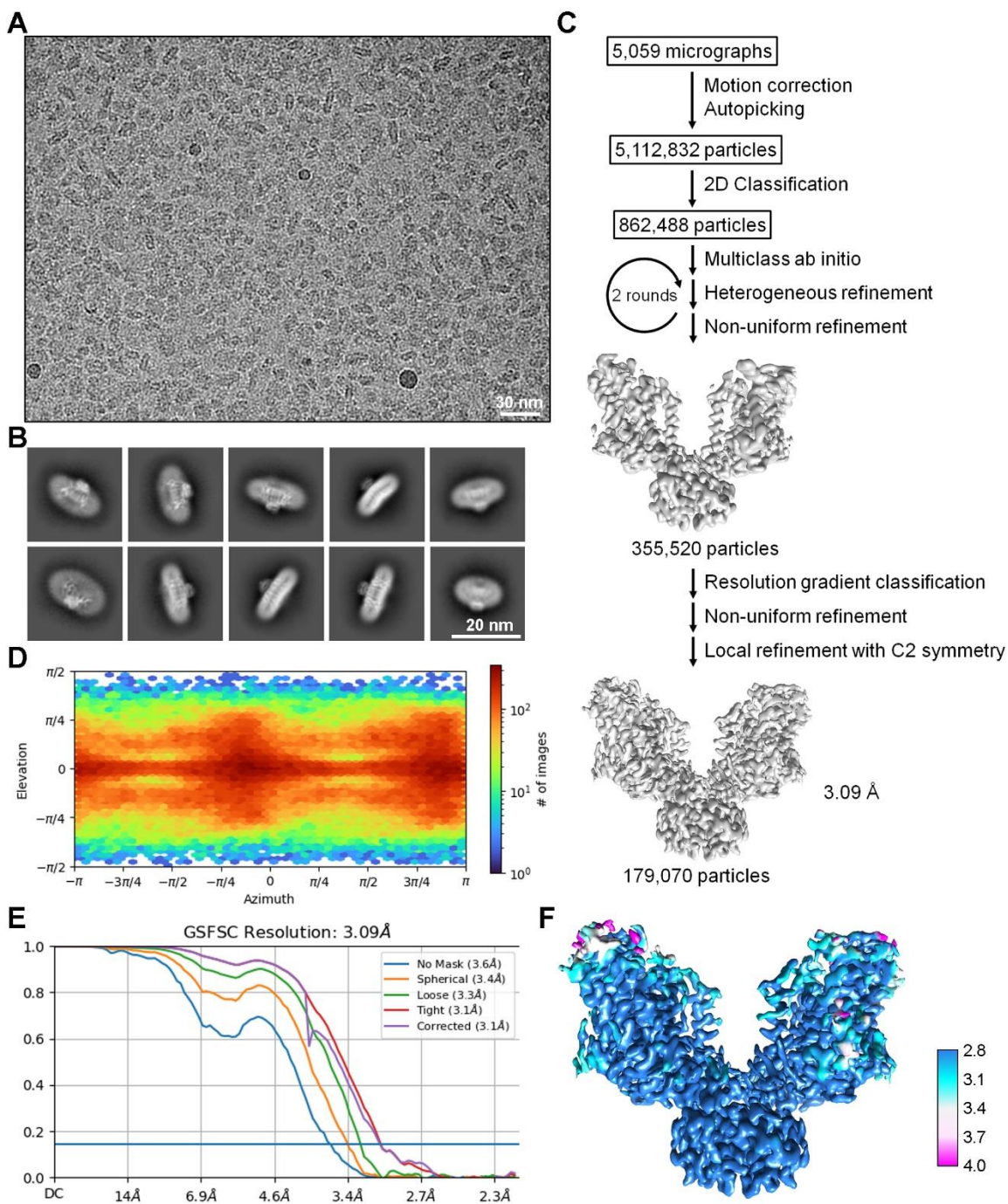
Structure and mechanism of a eukaryotic ceramide synthase complex

Tian Xie, Qi Fang, Zike Zhang, Yanfei Wang, Feitong Dong, and Xin Gong*

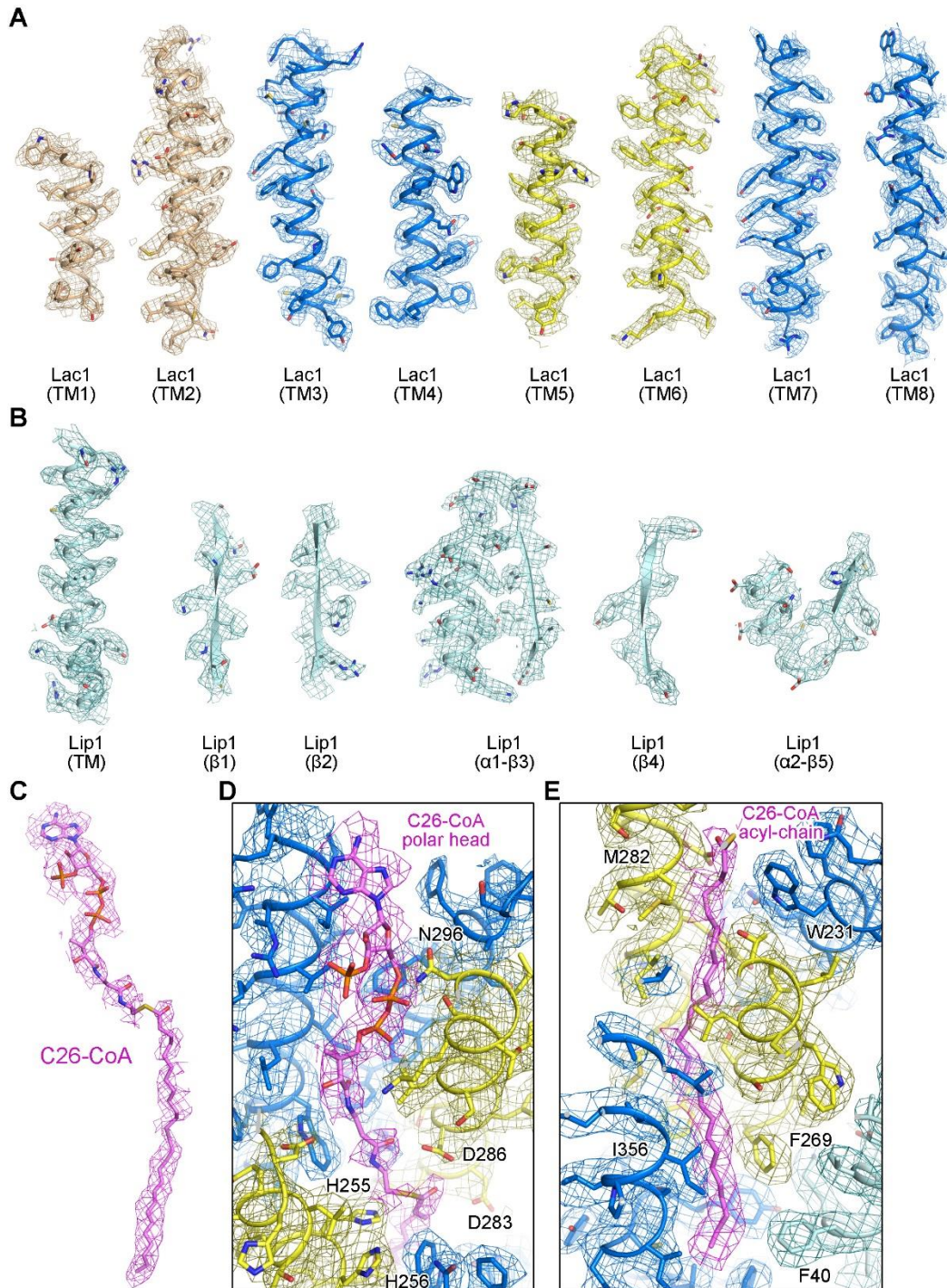
*To whom correspondence should be addressed: X.G. (gongx@sustech.edu.cn).

Table of contents

Contents	Page
Appendix Figure S1 Cryo-EM analysis of the C26-CoA-bound Lac1-Lip1 complex.	2
Appendix Figure S2 Representative density maps of the C26-CoA-bound Lac1-Lip1 complex.	3
Appendix Figure S3 Purification of C26-CoA binding mutants.	4
Appendix Figure S4 Characterization of Lac1-Lip1 mutants.	5
Appendix Figure S5 Cryo-EM analysis of the Lac1-Lip1 ^{S74F} complex.	6
Appendix Figure S6 Lac1-mediated oligomerization of the Lac1-Lip1 complex.	7
Appendix Table S1 Cryo-EM data collection, refinement, and validation statistics.	8



Appendix Figure S1 | Cryo-EM analysis of the C26-CoA-bound Lac1-Lip1 complex. **A**, Representative cryo-EM micrograph. **B**, Representative 2D class averages. **C**, Flowchart for cryo-EM data processing. **D-F**, Euler angle distribution, gold-standard FSC curves, and local resolution map of the C26-CoA-bound Lac1-Lip1 complex.

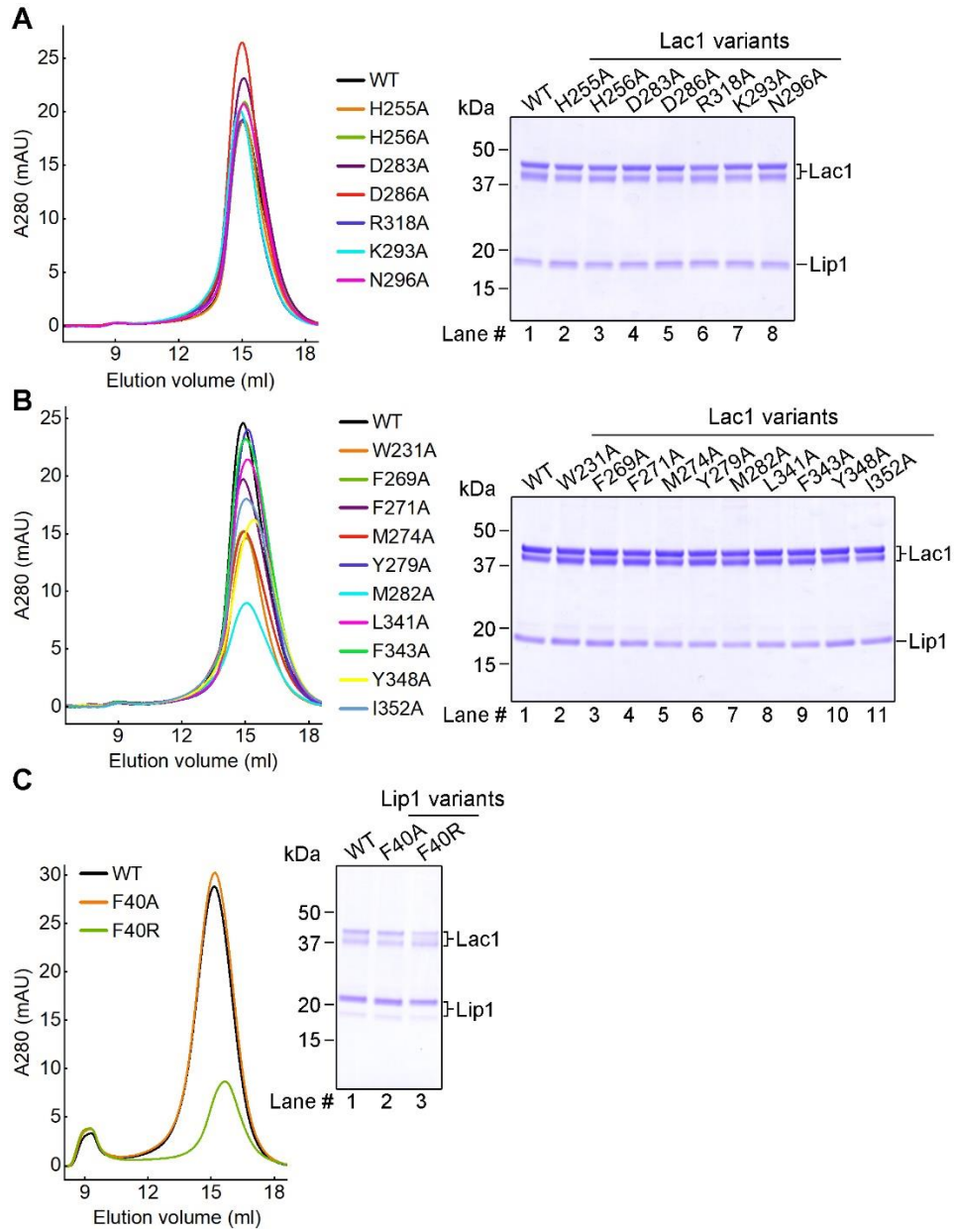


Appendix Figure S2 | Representative density maps of the C26-CoA-bound Lac1-Lip1 complex.

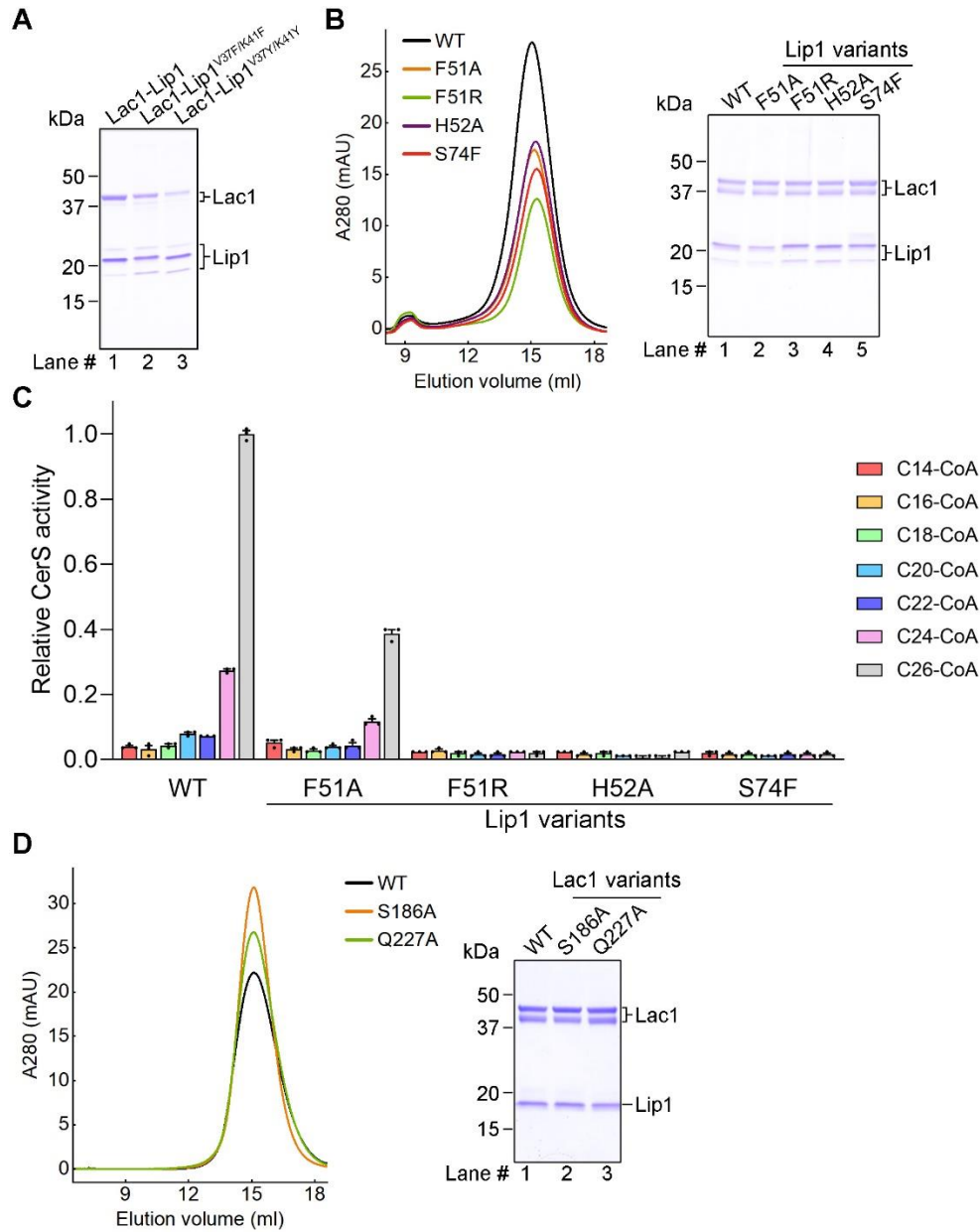
A-B, EM density maps of the representative secondary structural elements from Lac1 (**A**) and Lip1 (**B**).

C, Density map for C26-CoA. **D-E**, Close-up views of the density map for C26-CoA-binding sites.

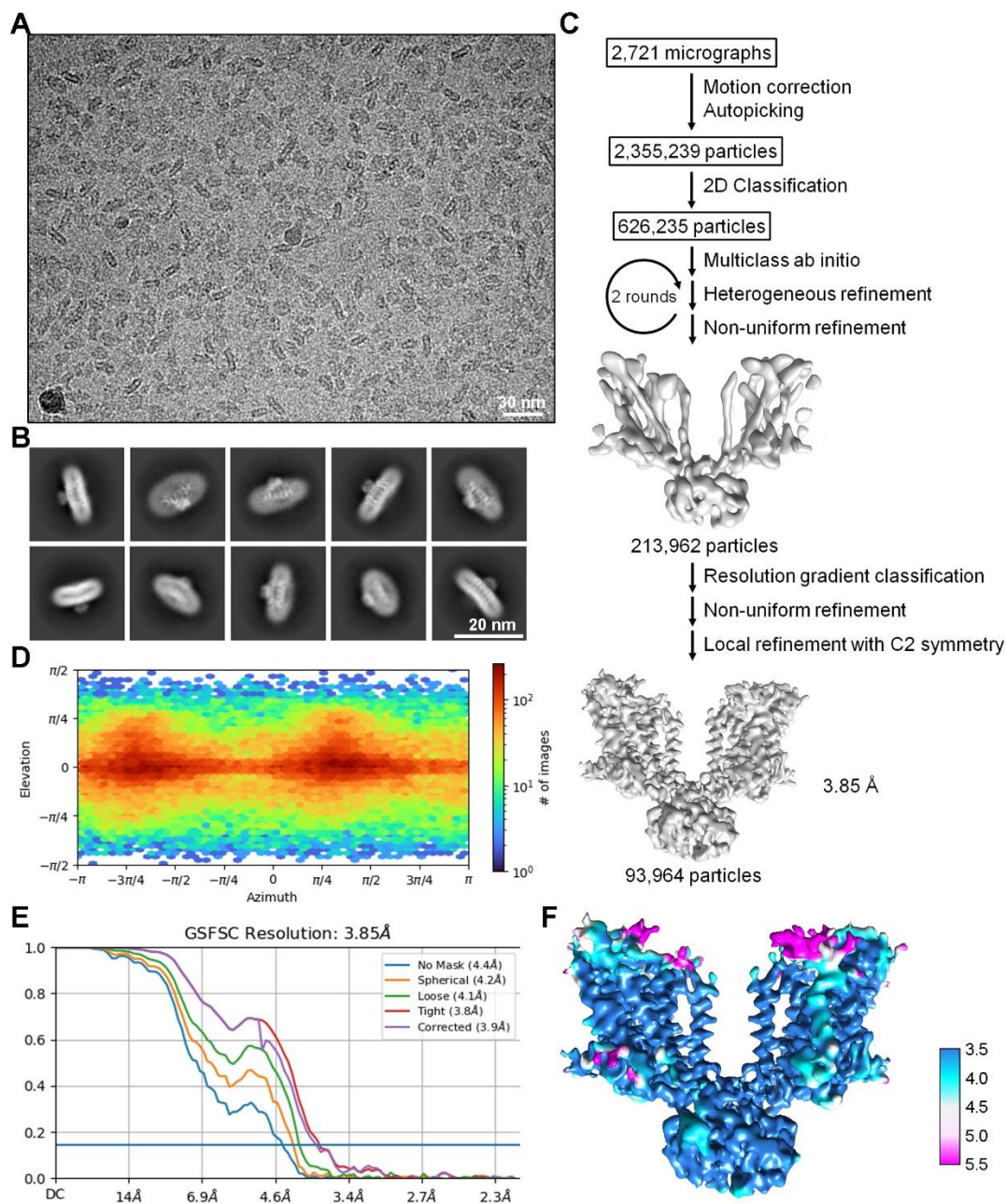
The density maps for C26-CoA were contoured at 3σ . All the other density maps were contoured at 5σ .



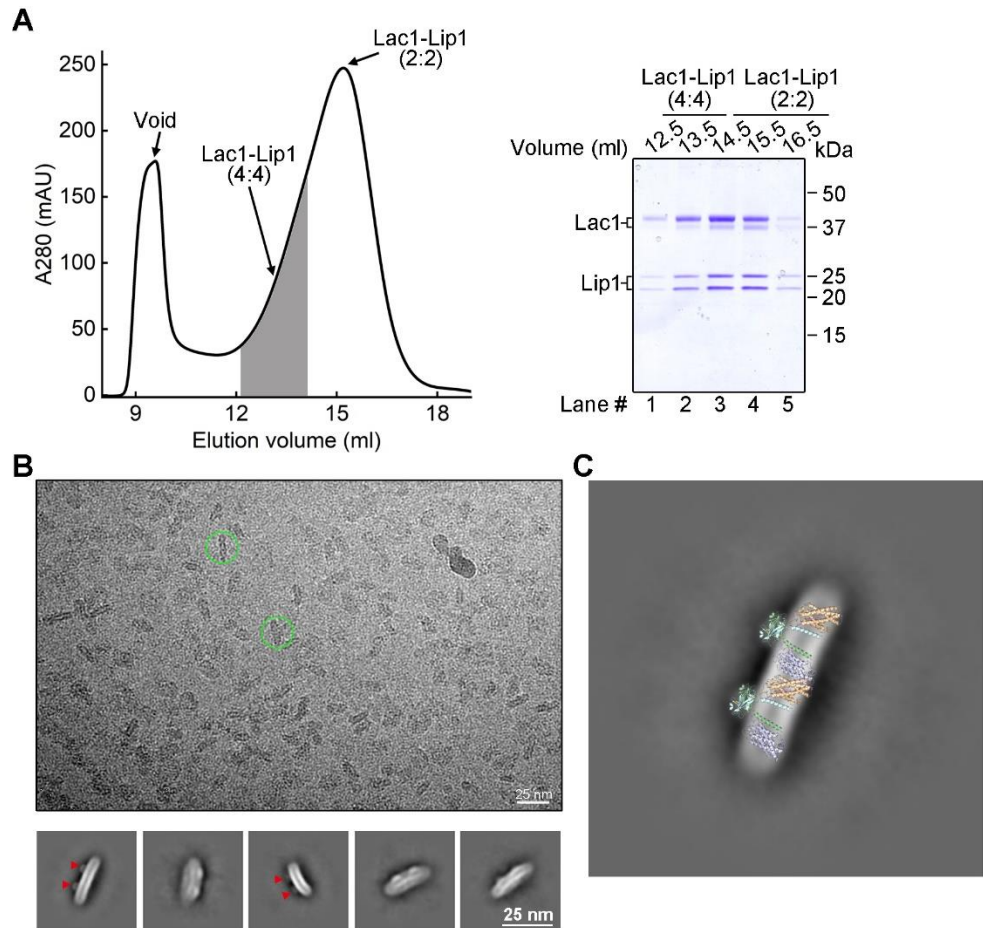
Appendix Figure S3 | Purification of C26-CoA binding mutants. SEC profiles and Coomassie blue-stained SDS-PAGE gels for the Lac1 hydrophilic cavity mutants (**A**), the Lac1 acyl-chain binding site mutants (**B**), and the Lip1 acyl-chain binding site mutants (**C**). Similar amounts of purified proteins were subjected to SDS-PAGE gels for analysis.



Appendix Figure S4 | Characterization of Lac1-Lip1 mutants. **A**, The Lip1 TM interaction interface mutants partially impaired the complex formation between Lac1 and Lip1. **B**, SEC profiles and Coomassie blue-stained SDS-PAGE gel for the Lip1 luminal interaction interface mutants. **C**, Acyl-chain selectivity of the Lip1 luminal interaction interface mutants revealed by CerS activity. Each data point is the average \pm SEM of three independent experiments. **D**, SEC profiles and Coomassie blue-stained SDS-PAGE gel for the Lac1 lateral-opening mutants. Similar amounts of purified proteins were subjected to SDS-PAGE gels for analysis in panels (**B**) and (**D**).



Appendix Figure S5 | Cryo-EM analysis of the LacI-Lip1^{S74F} complex. **A**, Representative cryo-EM micrograph. **B**, Representative 2D class averages. **C**, Flowchart for cryo-EM data processing. **D-F**, Euler angle distribution, gold-standard FSC curves, and local resolution map of the LacI-Lip1^{S74F} complex.



Appendix Figure S6 | Lac1-mediated oligomerization of the Lac1-Lip1 complex. **A**, SEC profile of a representative large-scale Lac1-Lip1 complex preparation. The major peak indicates the Lac1-Lip1 (2:2) complex as verified by cryo-EM analysis in Appendix Figure S1. Protein in the shoulder area before the Lac1-Lip1 (2:2) peak was collected for cryo-EM study and verified as Lac1-Lip1 (4:4) complex. **B**, Representative cryo-EM micrograph and 2D averages of the protein sample from the shoulder area. The typical Lac1-Lip1 (4:4) complex particles are indicated by green circles. The two Lip1 dimers are marked with red arrowheads. **C**, The representative 2D class average of the protein sample from the shoulder area can match well with the structures of two 2:2 Lac1-Lip1 complexes, revealing a potential Lac1-mediated oligomerization interface.

Appendix Table S1 | Cryo-EM data collection, refinement, and validation statistics.

	C26-CoA-bound Lac1-Lip1 complex (EMD-35862, PDB 8IZD)	Lac1-Lip1 ^{S74F} complex (EMD-35863, PDB 8IZF)
Data collection and processing		
Magnification	81,000	81,000
Voltage (kV)	300	300
Electron exposure (e ⁻ /Å ²)	50	50
Defocus range (µm)	-2.0 to -1.0	-2.0 to -1.0
Pixel size (Å)	1.072	1.072
Symmetry imposed	C2	C2
Initial particle images (no.)	5,112,832	2,355,239
Final particle images (no.)	179,070	93,964
Map resolution (Å)	3.09 Å	3.85 Å
FSC threshold	0.143	0.143
Map resolution range (Å)	2.8-4.0 Å	3.5-5.5 Å
Refinement		
Initial model used (PDB code)	None	None
Model resolution (Å)	3.1 Å	3.9 Å
FSC threshold	0.143	0.143
Model resolution range (Å)		
Map sharpening <i>B</i> factor (Å ²)	-117.8	-162.5
Model composition		
Nonhydrogen atoms	7,782	7,594
Protein residues	894	894
Ligands	8	2
<i>B</i> factors (Å ²)		
Protein	52.04	76.45
Ligand	52.21	69.24
R.m.s. deviations		
Bond lengths (Å)	0.005	0.005
Bond angles (°)	1.224	0.891
Validation		
MolProbity score	2.02	2.23
Clashscore	11.29	15.54
Poor rotamers (%)	0.00	0.00
Ramachandran plot		
Favored (%)	93.00	90.52
Allowed (%)	7.00	9.03
Disallowed (%)	0.00	0.45